Title
Structural and mechanistic aspects of carotenoid cleavage dioxygenases (CCDs)

Journal
Biochimica et Biophysica Acta (BBA) - Molecular and Cell Biology of Lipids, 1865(11)

ISSN
1388-1981

Authors
Daruwalla, Anahita
Kiser, Philip D

Publication Date
2020-11-01

DOI
10.1016/j.bbalip.2019.158590

Peer reviewed

Published in final edited form as:

Biochim Biophys Acta Mol Cell Biol Lipids. 2020 November ; 1865(11): 158590. doi:10.1016/j.bbalip.2019.158590.

Structural and Mechanistic Aspects of Carotenoid Cleavage Dioxygenases (CCDs)

Anahita Daruwalla[1,2], **Philip D. Kiser**[2,3,4]

[1.]Department of Pharmacology, Case Western Reserve University, Cleveland, OH 44106

[2.]Department of Physiology & Biophysics, University of California, Irvine, CA 92697

[3.]Research Service, VA Long Beach Healthcare System, Long Beach, CA 90822.

Abstract

Carotenoid cleavage dioxygenases (CCDs) comprise a superfamily of mononuclear non-heme iron proteins that catalyze the oxygenolytic fission of alkene bonds in carotenoids to generate apocarotenoid products. Some of these enzymes exhibit additional activities such as carbon skeleton rearrangement and *trans-cis* isomerization. The group also includes a subfamily of enzymes that split the interphenyl alkene bond in molecules such as resveratrol and lignostilbene. CCDs are involved in numerous biological processes ranging from production of light-sensing chromophores to degradation of lignin derivatives in pulping waste sludge. These enzymes exhibit unique features that distinguish them from other families of non-heme iron enzymes. The distinctive properties and biological importance of CCDs have stimulated interest in their modes of catalysis. Recent structural, spectroscopic, and computational studies have helped clarify mechanistic aspects of CCD catalysis. Here, we review these findings emphasizing common and unique properties of CCDs that enable their variable substrate specificity and regioselectivity.

Keywords

Non-heme iron; beta-propeller; nitric oxide; resveratrol; dioxetane; monotopic membrane protein

Introduction

While it has been known for nearly a century that β-carotene can serve as a precursor of vitamin A (retinol) in animals [1], the discovery and characterization of enzymatic activities that catalyze carotenoid cleavage has been a long process and remains an active area of research. A water soluble enzyme from rat liver and small intestine that cleaved β-carotene

[4.]Corresponding Author: Department of Physiology and Biophysics, School of Medicine, University of California, Irvine, 837 Health Sciences Road, Irvine, CA 92617. pkiser@uci.edu. Phone: (949) 824-6954.

Declaration of interests

The authors declare that they have no known competing financial interests or personal relationships that could have appeared to influence the work reported in this paper.

to form two molecules of retinaldehyde in the presence of O_2 was first described in 1965 [2, 3]. This enzyme was molecularly cloned from *Drosophila* and several vertebrate species in the early 2000s [4-8] following the identification of a plant 9-*cis*-epoxycarotenoid dioxygenase (NCED) known as viviparous-14 (VP14) [9]. Shortly thereafter, a second carotenoid oxygenase was identified that catalyzed excentric carotenoid cleavage [10]. It was also realized that these carotenoid cleaving enzymes exhibit sequence similarity to bacterial enzymes that oxidatively cleave the interphenyl double bond of lignostilbene [11, 12]. We now know that these enzymes constitute a superfamily of proteins that in general catalyze the oxygenolytic fission of conjugated alkenes in carotenoids and stilbene-like compounds (Fig. 1). This activity is critical for a number of biological processes including hormone signaling and light sensation and also contributes to production of aesthetically pleasing compounds in plants including those responsible for the smell of roses [13] and the color and aroma of saffron [14]. It is increasingly appreciated that these enzymes are not necessarily one-trick ponies, with some being capable of catalyzing “accessory” reactions that involve double bond isomerizations [15] and carotenoid carbon backbone rearrangements [16]. And in at least one case, oxidative cleavage is not the major biological reaction catalyzed, namely the retinal pigment epithelium-specific 65 kDa protein (RPE65) subfamily, which is critically involved in vertebrate visual function [17, 18]. Over the years, these enzymes have come to be known by a number of different names that reflect their particular substrate specificities or mechanistic features. For simplicity and to emphasize their evolutionary relatedness, we refer to these enzymes as carotenoid cleavage dioxygenases (CCDs) throughout this article.

CCDs exhibit characteristics that are invariant with respect to substrate specificity or catalytic activity. The defining sequence feature of these enzymes is the presence of four His and three Glu (or less commonly Asp) residues that function cooperatively to coordinate an Fe^{II} cofactor that is essential for catalytic activity. These residues reside in islands of relatively high sequence conservation that mark CCDs as being homologous despite the finding that paralogous sequences often exhibit low overall amino acid-level identity (Fig. 2A). The basic CCD fold was revealed in 2005 with the crystallographic structure determination of a retinal-forming CCD from *Synechocystis sp*. PCC 6803 [19]. The fold consists of a 7-bladed beta propeller covered on its top face by a helical “dome” that comprises most of the substrate binding pocket (Figs. 2B and 3). The iron cofactor is located on the top face of the propeller structure and is directly coordinated by the four invariant His residues, three of which are stabilized by three second-sphere Glu residues via hydrogen bonding interactions. At the time this structure was determined, it was suggested that the beta propeller moiety would be structurally preserved across the CCD superfamily whereas variations in the helical dome could account for differences in catalytic function between these enzymes [19]. Now that structures of several diverse CCDs have been determined, the truth of this statement has largely been confirmed. However, the active site plasticity of these enzymes is perhaps even greater than originally imagined. Indeed, the CCD structure possesses fold polarity – a rigid core beta propeller fold juxtaposed with a cluster of non-contiguous helical and loop segments of greater sequence variability and conformational flexibility – that is in general conducive to evolution of new activities and substrate

specificities [20, 21]. Additionally, it is becoming clear that alterations in the beta propeller structure are an important determinant of CCD quaternary structure.

It is noteworthy that the CCD iron center is structurally atypical compared to most other mononuclear non-heme iron oxygenases. It has been found that a large number of non-homologous proteins have structurally converged to bind iron through a 2-His/1 carboxylate (Glu or Asp), or more rarely 3-His, facial triad motif [22] providing a three coordination site anchor to the iron. The remaining sites are occupied by aquo/hydroxo ligands, which are typically displaced by substrates during catalysis. By contrast, CCDs coordinate iron only using His residues, and the active site of most of these enzymes is structured to disfavor 6-coordinate octahedral geometry.

The unusual active site features of CCDs coupled with their diversity in substrate specificity, regioselectively, and catalytic activity have motivated interest in studying mechanistic enzymology among the diverse members of this superfamily. These studies have been further driven by the opportunities afforded by a deep understanding of enzymatic mechanisms to develop specific inhibitors of CCDs for use in agriculture and medicine. The past ten years has witnessed major progress in the structural and enzymatic characterization of CCDs from diverse organisms. Several excellent reviews covering CCD substrate specificity and biological functions are available [e.g. 23, 24-29]. Here, we provide an update on CCD structure and mechanism with emphasis on the commonalities and diversity among this enzyme superfamily building upon prior reviews of the subject [30-33].

Synechocystis apocarotenoid-15,15’-oxygenase (ACO)

Introduction

Eubacteria, particularly cyanobacteria, have been studied extensively for their carotenoid and retinoid-cleaving activities [reviewed in 28]. Excentric β-carotene cleaving activity was originally identified in the cyanobacterium *Microcystis*, which generated two molecules of β-cyclocitral and one molecule of di-apo-carotenal crocetindial from beta-carotene [34]. The first eubacterial carotenoid-cleaving CCD to be cloned and characterized was from *Synechocystis* sp. PCC 6803, a unicellular, freshwater cyanobacterium that encodes two CCD proteins (ORFs: *sll1541 and slr1648*), referred to as Diox1 and Diox2 [35, 36]. *In vitro* expression and enzymatic analysis of Diox1 subsequently showed its inability to cleave full-length carotenoids, with activity instead towards apocarotenoids and apolycopenals [35]. Intriguingly, Diox1 generated retinal from apocarotenoids, making it the first prokaryotic enzyme identified to display this activity. Known today as apocarotenoid-15,15’-oxygenase (ACO), it cleaves at the 15-15’ double bond of the all-*trans* form of β-apo-8’-carotenal to produce retinal (C_{20}) and a smaller (C_{10}) molecule, apo-8’-15-apo-carotene-dial. Another cyanobacterium *Nostoc* sp. PCC 7120 was also found to encode CCDs in its genome that catalyze central and excentric cleavage of apocarotenoids and carotenoids [37] as well as neurosporenes and torulenes [38]. Retinal is known to be critical for photoreception, growth and stress responses in these bacteria, but much remains to be learned about the physiological relevance of CCD activity in microorganisms.

Sequence, topology and overall structure:

ACO was the first member of the CCD superfamily to be studied by X-ray crystallography and remains the prototypical structure to which other CCDs are compared [19]. As described above the structure consists of a seven-bladed β-propeller core with four His residues at the propeller axis forming the iron cofactor-binding site. Five of the seven blades consist of classical four anti-parallel strands with blades 1 and 7 being five stranded as a result of an *N*-terminal sequence extension (Fig. 2B). The bottoms of the propeller blades are generally connected by short loops as opposed to their tops which feature extended segments that coalesce into dome-forming loops and alpha helices (Fig. 3). The exterior of the ACO molecule features a hydrophobic patch consisting of Trp, Phe, Ile and several Leu residues as well as a few positively charged Lys and Arg residues that together confer the ability of this protein to interact in a monotopic fashion with membranes [39] where its lipophilic carotenoid substrates are naturally found [40]. Interestingly, despite the presence of this hydrophobic patch, ACO behaves to a large extent like a soluble protein during purification, although detergents are required for its crystallization [19].

Metal Center:

ACO crystal structures feature average Fe-Nε bond lengths of 2.1-2.2 Å. In its resting state, the Fe^{II} ion is coordinated by five ligands arranged in a square pyramidal geometry (Fig. 4A). These are the four conserved His residues (183, 238, 304 and 484) mentioned above in addition to a single solvent atom bound *trans* to His183. The site *trans* to His304 is occluded by the methyl group of Thr136, and no ligand electron density has been observed at this site in ACO crystal structures determined to date [19, 41]. Interestingly, mutation of Thr136 to Ala was not sufficient to allow binding of two solvent molecules but did cause the solvent to shift position giving the iron a distorted trigonal bipyramidal structure [42]. These crystallographic results were corroborated by X-ray absorption spectroscopy (XAS) studies which confirmed a five-coordinate Fe^{II} resting state with average Fe-Nε bond lengths of 2.15 Å [43]. ^{57}Fe Mössbauer spectroscopy analysis further demonstrated that the iron center in ACO, as isolated using standard aerobic purification methods, is in the high-spin Fe^{II} state with isomer shift and quadrupole splitting parameters similar to other mononuclear non-heme iron proteins [43]. These findings demonstrate the unusual resistance of ACO to auto-oxidation and also indicate that the 4-His coordination motif does not markedly alter the iron electronic structure relative to the environment provided by the facial triad coordination motif. His 238, 304 and 484 are involved in hydrogen bonding interactions with Glu residues 150, 370, and 426. These hydrogen bonding interactions play an important role in stabilizing the conformation of the His residues as demonstrated by Glu150 mutagenesis experiments [44]. Notably, the iron ion can be substituted with Co^{II} added during protein expression to give a catalytically inactive but isostructural form of the enzyme [45].

Active site tunnel:

A tunnel extends from the outside of the protein at the hydrophobic patch onto the active Fe^{II} center and ends at Leu400 (Fig. 4B). This region resides at the junction between the propeller and helical cap regions of the structure and is roughly perpendicular to the propeller axis. It is lined with several aromatic and nonpolar side chains allowing the tunnel

to function as a passageway for extraction of lipophilic apocarotenoids from the membrane. These residues may control substrate specificity and reactivity as well as stabilize reaction intermediates through a number of mechanisms including π stacking, quadrupole, and *van der Waals* interactions. The structure also features a second tunnel, continuous with the first, that was suggested to act as an exit site for smaller, more hydrophilic apocarotenoid products. In their study, Kloer *et al*. reported the presence of a bent electron density feature in the ACO active site that was attributed to the substrate, (3*R*)-3-hydroxy-8'-apocarotenol, which was added during a crystal soaking experiment [19]. This density was in the form of a cranked rod that could only be filled by modeling the substrate in a 13,14-13',14'-di*cis* configuration. It was therefore speculated that the enzyme had isomerized the substrate prior to the cleavage reaction. In a follow-up study by Sui *et al*. [41], it was found that ACO, crystallized as in the original study in the presence of the detergent C_8E_6 but without added substrate, exhibited electron density nearly identical to that reported by Kloer *et al*. [19]. This observation together with biochemical and spectroscopic analyses, ruled out isomerase activity for ACO and indicated that the density attributed to substrate was in fact due to a bound detergent or precipitant molecule. Indeed, the addition of linear polyoxyethylene detergents strongly inhibited the activity of ACO indicating that such detergents can competitively inhibit substrate binding [41].

Substrate specificity and mutagenesis studies:

Ruch *et al*., showed *in vitro* activity of ACO towards all-*trans*-β-apo-8'-carotenal, all-*trans*-β-Apo-8'-carotenol and their corresponding hydroxyl ring variants as well as all-*trans*-(3*R*)-3-OH-β-apo-12'-carotenal. In each case the enzyme generated retinal (or 3-hydroxyretinal) as a product by cleaving at the C15-C15' double bond. Activity was higher for all-*trans*-β-apo-8'-carotenol and its hydroxy derivatives in comparison to the corresponding aldehydes. It also favored substrates with chain length from C25 to C35, with shorter chains having reduced cleavage rates. To examine the role of select active site residues in substrate binding and cleavage, Sui et al., performed mutagenesis experiments based on an *in silico* substrate-docked model of ACO. One focus was on three hydrophobic residues ($Trp^{-}149$, Phe113, Phe236) located near the entrance to the active site cavity that were postulated to play a role in substrate recognition by creating a bottleneck near this entrance [19]. This bottleneck hypothesis was used to explain the inability of ACO to metabolize full-length carotenoids. A regio-selective C15-C15' cleavage site is facilitated by the proximal phenyl rings of Phe69 and Phe303. The kink-like arrangement prevents entry of the substrate β-ionone ring, and enables the terminal hydroxyl moiety to interact with Tyr24 at the distal end pocket. Individual point mutations of these bottleneck residues reduced catalytic activity but did not affect substrate regio-selectivity, indicating that cleavage selectivity is enforced by multiple residues. Crystallographic studies on a Trp149 mutant revealed that this site is also important for maintaining the interaction between His238 to Glu150, demonstrating that active site substitution can exert long-range effects on the catalytic center [44]. This finding emphasizes the importance of the His-Glu, two sphere arrangement around the iron center in maintaining activity.

Mechanistic studies

The catalytic mechanism of ACO has been studied through computational quantum chemistry [46] using a model of ACO in complex with (3*R*)-hydroxy-apo-8'-carotenol, derived from crystallography [19]. Although the calculations relied on a model of an ACO-carotenoid complex that was later found to be not fully supported by experimental data [41], this study has nevertheless provided important insights into the reaction mechanism as well as hypotheses for experimental testing. The study investigated mechanisms involving both dioxetane and epoxide intermediates [32] in the presence and absence of an iron-coordinated water molecule. Given the absence of water coordination to the sixth coordination site, which is enforced by the methyl group of Thr136, the mechanism in which O_2 binding is accompanied by release of water is most probable and is presented in Fig. 5. Additionally, the close proximity of O_2 and the carotenoid in the ternary complex is supported by electron paramagnetic resonance (EPR) studies on the ACO iron complex with nitric oxide (NO), an O_2 mimetic, which showed that its electronic structure is substantially perturbed in the presence of apocarotenoid [43]. In this mechanism, side-on binding of O_2 to the Fe^{II} center is energetically most favorable and is accompanied by electron transfer from the carotenoid substrate to form an Fe^{II}-O_2^- - apocarotenoid radical cation intermediate that is presumably stabilized by resonance delocalization. Notably, this concurrent electron transfer from carotenoid to the Fe-O_2 complex suggests a mechanism by which activated O_2 is only generated in the presence of carotenoid substrate. α→β inversion of the carotenoid unpaired electron leads to a reactive quintet spin state. The activated oxygen species undergoes nucleophilic attack on the C15 carbocation together with free radical spin recombination to form the dioxetane intermediate. O-O bond rupture is facilitated by its interaction with Fe^{II} whereby an Fe^{III}-diolate radical is transiently formed followed by decay to yield the final apocarotenoid products with iron restored to the 2+ oxidation state. Notably the absence of water in the first coordination sphere of iron was found to prohibit a mechanism involving an epoxide intermediate. The rate-limiting step of the dioxetane mechanism was found to be the initial attack of activated oxygen on the 15-15' bond of the apocarotenoid substrate. The overall reaction is calculated to be highly exergonic as expected. Notably, the model used for the computations did not include the Thr136 residue that is closely situated to the iron center and likely influences O_2 binding to iron center. A key prediction of the study was that the ACO-catalyzed carotenoid cleavage reaction occurs via a dioxygenase-based mechanism, which was later confirmed through well-controlled oxygen-labeling experiments conducted by Sui and colleagues [42].

Zea mays VP14 and other plant CCDs

Introduction:

About thirty years after the discovery of β-carotene-cleaving enzymes in animals, the first plant carotenoid-cleaving enzyme was isolated from *Zea mays* [9]. Known as viviparous-14, the encoding gene was cloned from a strain of maize exhibiting seed vivipary owing to a deficit in the phytohormone, abscisic acid. This CCD belongs to the NCED group, a subfamily required for synthesis of xanthonin, the precursor of abscisic acid (Fig. 1A). VP14 was recognized as a homolog of lignostilbene dioxygenase (LSD) from *Pseudomonas paucimobilis* as well as vertebrate RPE65 [12]. The sequence of this enzyme enabled

identification of metazoan CCDs [7] as well as numerous other carotenoid-metabolizing enzymes in plants [25].

Plant CCDs phylogenetically cluster into four other sub-families which each display characteristic substrate specificities and regioselectivities (Fig. 1A). CCD1 enzymes cleave a variety of linear and cyclic carotenoids at variable positions to produce apocarotenoids involved in flavor and fragrances [47, 48]. *Crocus sativus* CCD2 cleaves zeaxanthin at the 7-8 and 7'-8' positions to form crocetin dialdehyde and 3-hydroxy-β-cyclocitral – precursors of apocarotenoids responsible for the color and aroma of saffron [14]. CCD4 enzymes cleave carotenoids asymmetrically and contribute to coloration in plant tissues such as *Chrysanthemum morifolium* [49] and *Brassica napus* [50] petals, potato tubers [51] and *Citrus* peels [52], whereas CCD7 and CCD8 are involved in the synthesis of the strigolactone precursor, carlactone, from 9-*cis*-β-carotene [16]. To date, VP14 is the only plant CCD for which high resolution structural information is available [53]. Below, we focus our discussion on this enzyme as well as advances made in understanding catalysis by CCD1 and CCD8.

Sequence, topology and overall structure.

VP14 is a 604 amino acid protein that contains an *N*-terminal chloroplast-targeting transit peptide sequence that has been described as consisting of residues 1-43 [12] or 1-75 [53]. The signal sequence is followed by an alpha helical region not found in ACO that is amphipathic and in part mediates binding of VP14 to the stromal side of thylakoid membranes [54] (Fig. 2B). Excluding the *N*-terminal signal peptide region, VP14 is about 26% identical to ACO, with regions of higher similarity surrounding the conserved iron binding residues as well as other catalytically important residues (Fig. 2A). It shows 60-85% identity to NCEDs from other plants while similarity to more distantly related plant CCDs is variable, ranging from 16-58% identity to *Zea mays* CCD1 and CCDs from *Arabidopsis* [53]. The fold topology of VP14 is highly similar to that of ACO (Fig. 2B). The structure of the loop regions on the bottom face of the beta-propeller are similarly well conserved, whereas the loops and helices capping the top face are highly divergent in sequence and structure between the two proteins [30]. VP14 features a disulfide bridge connecting the inner two strands of propeller blade 4, which is a unique feature among CCDs of known structure.

Active site and membrane penetration.

The iron cofactor is coordinated by four His residues (His298, His347, His412 and His590) on the innermost strands of blades 1, 3, 4 and 5 with average Fe-N_ε bond lengths of ~1.9 Å (Fig. 6A), which is significantly shorter than Fe-His bond lengths found for other CCDs and may have been enforced by bond restraints imposed during refinement as a result of the low resolution of the data. The fifth and sixth coordinating sites were modeled with a water molecule *trans* to His412 and an end-on bound O_2 molecule *trans* to His298, respectively. The apparent binding of oxygen in the absence of organic substrate is unusual for mononuclear non-heme iron proteins [55]. Given the limited resolution of the structure, the placement of O_2 at this position in the organic substrate-free state should be interpreted cautiously. In light of structural and spectroscopic studies on other CCDs, it is likely that O_2

does in fact bind *trans* to His298 although a side-on binding mode is also possible. Second sphere Glu residues 264, 477 and 530 are hydrogen bonded to His residues 347, 412 and 590, respectively (see footnote 1). As in ACO, a tunnel runs past the Fe^{II} center all the way to the other side of the protein, suggesting that the organic substrate and products could enter and leave the active site through distinct openings (Fig. 6B). Also, like other carotenoid-cleaving CCDs, VP14 has a hydrophobic patch at its exterior. This ~2,226 $Å^2$ patch is composed predominantly of two anti-parallel helices (α-1 and α-3) from residues 88-108 and 222-237. These regions generate a surface composed mainly of Leu, Ala, Phe, and Val side chains that are capable of penetrating to the interior of the membrane allowing interaction with the hydrophobic acyl chains (Fig. 6B). The patch also features some positively charged residues within and nearby the loop region of α-1, which could further promote membrane affinity via interactions with negatively charged lipid head groups. This amphipathic α-1 helix is essential for VP14 interaction with the thylakoid membrane as disruption of these residues leads to loss of abscisic acid synthesis [54], probably due to its inability to reach the lipophilic substrate. Helix α-3 is also adjacent to the substrate entry site, lined by hydrophobic aromatic residues. The favorable free energy of VP14 insertion into a model membrane led the investigators to postulate that VP14 penetrates the thylakoid membrane using its hydrophobic patch, bringing the substrate entry tunnel in close proximity to membrane-dissolved 9-*cis*-epoxy-carotenoids [53]. *In vitro* activity assays require inclusion of detergent such as Triton X-100 for efficient carotenoid cleavage to be observed [9]. Despite the rather large hydrophobic surface present in VP14, this protein can be purified and crystallized in the absence of detergent or other lipid mimetics [53]. Inspection of the VP14 crystal packing arrangement reveals that the hydrophobic faces pack together as trimers to partially shield each other from the aqueous solvent. The question of whether VP14 forms such trimers in detergent-free aqueous buffers has not been addressed but the ability of such structures to form may explain why a portion of VP14 is found to be soluble *in vivo* [54].

Substrate specificity and relationship to the VP14 active site:

VP14 and other NCEDs exhibit a fairly stringent substrate specificity, cleaving only 9-*cis*-isomers of xanthophylls including violaxanthin, neoxanthin, and zeaxanthin [9] (Fig. 1B). Cleavage of the first two substrates, which are the only physiologic 9-*cis*-carotenoids found in plants [56], gives rise to 9-*cis*-xanthoxin, a precursor of abscisic acid. The enzyme can tolerate fairly divergent structures on the end of the carotenoid opposite of the 9-*cis* side, although changes in this region can lead to non-productive substrate binding and poor cleavage efficiency as shown for isomers of 9-*cis*-luteoxanthin [56]. Although the structure of VP14 in complex with a 9-*cis* carotenoid substrate hasn't been determined, docking studies have provided hypotheses regarding the roles of active site residues in the cleavage reaction. These studies predict that substrates are extracted into the active site from the membrane with the 9-*cis* side of the carotenoid entering the active site first. The scissile

[1]Readers should note that there is a discrepancy between the description of the VP14 structure in reference [53] and the coordinates deposited in the Protein Data Bank (PDB accession code 3NPE) in the location of the Glu477, which is a part of the second sphere iron coordination motif. Images of the VP14 structure used in this manuscript were generated using a re-refined structure of VP14 in which the Glu477 residue is placed in its proper location forming a hydrogen bond with His 412. These updated coordinates are available upon request.

11,12 double bond is predicted to be held in position by the side chains of Phe 171, 411, and 589. This orientation readily explains the ability of VP14 to cleave carotenoids with diverse structures away from the 9-*cis* side of the molecules. The absence of residues near the scissile bond that could be involved in proton shuttling was interpreted as a favorable environment for a dioxetane-based mechanism [53].

Substrate specificity, mutagenesis, and isotope labeling studies on AtCCD1.

The discovery of VP14 paved the way to identification of other plant carotenoid cleaving enzymes, first among which was the enzyme from *Arabidopsis thaliana*, named CCD1. CCD1 is unique among plant CCDs in being the only enzyme that does not localize to plastids, instead being found in the cytosol [32, 57]. It was found to be a relatively promiscuous enzyme, cleaving a variety of carotenoids and apocarotenoids at the C-9,10 and C-9',10' positions, forming a C_{17}-dialdehyde and a smaller C_{13} product [58]. *In vivo* studies demonstrated that AtCCD1 mutants had an increased seed carotenoid content [57]. It was later discovered that ZmCCD1 as well as orthologs from other species of plants can cleave at additional double bond positions depending on the specific substrate [13, 47]. Based on these results, it was proposed that the cleavage site selectivity is determined by the saturation status between carbons 7 and 8 (7' and 8') and carbons 11 and 12 (11' and 12') as well as the methyl groups on carbons 5, 9, and 13 (5', 9', and 13') [47].

A homology model of ZmCCD1 constructed using the coordinates of the VP14 crystal structure revealed candidate residues involved in differences in substrate specificity [51]. Val478 residing on the innermost strand of blade VI in VP14 is substituted by a Phe409 in ZmCCD1, disrupting the cleft that houses the methyl group on C9 of the 9-*cis*-carotenoid and interferes with the alignment of C11-12 bond over the catalytic iron [51]. Secondly, the loop region at the back end of the substrate pocket formed by residues 499-503 and Leu170 in VP14 is substituted by residues 432-434 and a Trp104 in ZmCCD1. This disrupts the formation of a pocket that accommodates the second ring of 9-*cis*-epoxycarotenoids in VP14 and other NCEDs and is thought to be absent in the other CCDs as well. Lastly, three Phe residues, 171, 411 and 589 in VP14, known to be critical in substrate positioning and specificity are conserved in ZmCCD (residues 105, 343 and 533) and are important for enzyme activity. In addition, Ile147 proximal to Phe105 (Ile215 in VP14) in ZmCCD1 also is important for substrate cleavage, as seen by the reduced activity upon substitution to Ala.

The stoichiometry of O_2 incorporation into the products of β-apo-8'-carotenal cleavage by AtCCD1 was studied using recombinantly expressed protein [59]. Importantly, the β-ionone product of this reaction contains a ketone moiety which is much less prone to solvent oxygen back-exchange compared to aldehyde-containing products. In isotope-labeling experiments with $H_2{}^{18}O$, the GC-MS spectrum of β-ionone was similar to that obtained in unenriched water. However, when the reaction was performed in an $^{18}O_2$ atmosphere, almost all of the β-ionone (~96%) was labeled with the oxygen isotope. By contrast, only 27% of the other product, C_{17}-dialdehyde, carried an oxygen atom from O_2, reiterating the fact that ^{18}O contained in the nascent aldehyde products is readily lost and replaced with oxygen from the solvent, particularly under low pH conditions. Nevertheless, the observed labeling

of both products provided the first direct evidence that CCDs do in fact operate as dioxygenases.

Mechanism of carlactone formation by CCD8.

Strigolactones are C_{19} carotenoid derivatives with a tricyclic lactone structure connected to a second lactone ring via an enol ether bridge [16]. They inhibit branch tillering and are released by plant roots into the soil where they play a critical role in maintaining plant symbiosis with mycorrhizal fungi but also trigger seed germination of certain parasitic weeds [60]. CCD7 and CCD8 were identified as the CCDs involved in biosynthesis of carlactone, a monolactone strigolactone precursor, from 9-*cis*-β-carotene [16]. CCD7 first stereo-specifically cleaves 9-*cis*-β-carotene into 9-*cis*-β-apo-10'-carotenal and β-ionone. CCD8 then catalyzes oxygenation of 9-*cis*-β-apo-10'-carotenal to form carlactone. This step, however, involves an unusual rearrangement of the carbon backbone and potential mechanisms were only recently elucidated through isotope labeling experiments [60] and enzyme kinetic analysis [61].

CCD8 activity assays carried out in the presence of $^{18}O_2$ or $H_2{}^{18}O$ confirmed the incorporation of three O_2-derived oxygen atoms in carlactone and ruled out the presence of the substrate aldehyde oxygen [60]. These data demonstrated that CCD8, like CCD1 and ACO, acts as a dioxygenase. However, CCD8 consumes two molecules of O_2 during each round of catalysis unlike other characterized CCDs. The carlactone product is shorter than the apocarotenoid substrate by eight carbon atoms. Use of a carbonyl derivatization agent allowed identification of the second CCD8 reaction product as 7-hydroxy-4-methylheptatrienal [60]. Two mechanisms have been proposed to account for the dual oxidative cleavage reaction and backbone rearrangement catalyzed by CCD8. The first involves formation of two successive endoperoxide bridges between C11 and C14 of the substrate, which necessitates the substrate to adopt a 12-13 s-*cis* conformation for proper orientation of the carbon atoms [60]. The second mechanism involves two Criegee rearrangement steps each occurring after formation of an iron-peroxo bridge intermediate [61]. Both mechanisms predict that the chiral (*R*) acetal carbon found in the lactone ring of the product originates from C11 of the substrate, which was confirmed by a ^{13}C-nuclear magnetic resonance labeling experiment [60]. Both mechanisms also require the presence of an active site proton donor. By contrast, the Criegee rearrangement mechanism involves an active site nucleophile that may represent a Cys residue based on reaction inhibition by sulfhydryl modifying reagents [61]. The step at which the second product is released also differs between the two mechanisms. In light of the different active site requirements for the two proposed mechanisms, structural studies on CCD8 could be particularly helpful in resolving which is more likely.

Stilbene-cleaving CCDs

Introduction

Interestingly, the first alkene-splitting CCD to be molecularly cloned was not a carotenoid-cleaving enzyme but rather an LSD expressed by the bacterium *Sphingomonas paucimobilis* TMY1009, which was isolated from pulping waste sludge [11]. This protein was found to

cleave the interphenyl alkene bond of lignostilbene and other lignin model compounds that arise mainly during industrial lignin processing. Closely related enzymes have been identified in other bacteria such as *Novosphingobium aromaticivorans* DSM12444 and *Bradyrhizobium sp*. BTAi1 [62] and fungi such as *Neurospora crassa* [63] and *Ustilago maydis* [64] that can cleave other stilbenes such as resveratrol and its derivatives. Given that resveratrol is an important phytoalexin that helps combat diseases, it has been speculated that resveratrol-cleaving CCDs may help pathogenic organisms evade this plant defense system [64]. Recently it was found that stilbene-cleaving CCDs enable rhizospheric bacteria to use resveratrol as a sole carbon source [65, 66]. Because resveratrol and related compounds are less hydrophobic than typical carotenoids and therefore more amenable to biochemical and biophysical investigations carried out in aqueous solutions, stilbene-cleaving CCDs have been important model systems for study of the alkene-cleavage reaction.

Sequence, topology, and overall structure

The structural biology of stilbene-cleaving CCDs has advanced rapidly over the past four years with structure determinations of *N. sphingobium* oxygenase 1 (NOV1) [67], *N. crassa* oxygenase 1 (CAO1) [43], *Pseudomonas brassicacearum* LSD [68], and most recently LsdA from *S. paucimobilis* TMY1009 [69]. These enzymes share approximately 40-55% sequence identity with rare sequence-specific indels. The sequence lengths are thus conserved at about 490 residues, with the exception of CAO1 which contains an *N*-terminal extension that is disordered in the crystal structure. This relatively high sequence conservation translates into high structural similarity with overall RMS deviations between Cα atoms in the range of 1-1.7 Å [70]. Stilbene-cleaving CCDs adopt a fold topology similar to that of ACO (Fig. 2B).

Metal binding site

The metal binding sites of stilbene-cleaving CCDs exhibit high structural similarity to that of *Synechocystis* ACO. Iron is directly coordinated by 4 His residues with three of these involved in hydrogen bonding interactions with the 3 conserved Glu residues (Fig. 7A). The iron centers of most of these enzymes contain a single bound solvent molecule *trans* to the first conserved His (His197 in CAO1) and are therefore 5-coordinate. The one exception is the structure NOV1 where a dioxygen molecule was modeled in the equivalent site. However, the legitimacy of modeling dioxygen in this structure has been questioned [71]. Like in ACO, these structures all possess a Thr methyl group positioned close to the region *trans* to the third His ligand (His313 in CAO1), which appears to inhibit diffusible ligand (e.g. water or O_2) binding at this position. The geometry of metal binding in these enzymes is therefore best described as either square pyramidal or trigonal bipyramidal with iron-His bond lengths in the range of 2.1-2.2 Å. The structure of the metal center in solution has been evaluated by XAS, which revealed a five coordinate structure and metal-ligand bond lengths of 2.15 Å, in close agreement with XAS results obtained for *Synechocystis* ACO [43]. Despite this close structural similarity with ACO, ^{57}Fe Mössbauer spectroscopy has revealed greater electropositivity at the metal center of CAO1 compared to that of ACO, which is reflected in the lower isomer shift value for the former enzyme [43]. This finding suggests

that electron density transfer from Fe^{II} to O_2 upon their complexation could be reduced in CAO1 compared to ACO, which likely has catalytic consequences.

Active site cavity and residues that confer substrate specificity

The structure of the active site cavity of stilbene-cleaving CCDs represents a major point of divergence between these enzymes and carotenoid-cleaving CCDs. The active site entrance in stilbene-cleaving CCDs is located on nearly the oppose side of the helical dome compared to that of ACO and VP14 and does not traverse the structure, instead dead-ending near its center (Fig. 7B). The organic substrate-binding site, located adjacent to the metal center, is relatively narrow and flat, consistent with the expected planar structure of the stilbenoid substrates. The orientation of substrate binding was revealed by structures of Co-substituted CAO1 in complex with resveratrol and piceatannol [43] (Fig. 8). The substrate-binding cleft is predominantly lined by aromatic side chains that could serve to promote binding and stabilize reaction intermediates through *van der Waals*, pi stacking, and/or quadrupole interactions. Additionally, these structures revealed a pre-active site binding pocket closer to the surface of the protein where substrate may initially interact before moving to the site of catalysis. The innermost region of the substrate binding pocket is lined by Tyr and Lys side chains that interact with the 4'-hydroxyl group of stilbenoid substrate and are highly conserved among stilbenoid cleaving CCDs. Substitution of these residues in LsdA led to a dramatic decrease in catalytic activity supporting their key functional roles [69]. The conserved interactions involving these residues helps explain the absolute requirement for a 4'-hydroxy group in the substrates of stilbenoid cleaving CCDs [72].

Structures of stilbene-cleaving CCDs in complex with resveratrol and piceatannol have revealed the starting geometry of the stilbenoid cleavage reaction [43, 67] (Fig. 8). Substrate binds with slight distortion away from perfect planarity. This conformation is enforced by the geometry and electrostatic features of the binding site and may be an important factor in producing a more reactive electron density distribution. The substrate α-carbon is located ~4.7 Å away from the metal center and ~3 Å away from the solvent binding site. The substrate is thus well positioned for the cleavage reaction assuming that the solvent is eventually displaced by O_2 as the reaction progresses. The minimal interaction between organic substrate and the iron center suggested by these structures was corroborated by ^{57}Fe Mössbauer spectroscopy studies which showed nearly identical spectral characteristics between the enzyme and enzyme-substrate complexes [43].

Nitric oxide has been used as a surrogate for O_2 to study the binding of diatomic substrate to the iron centers of stilbene-cleaving CCDs in the presence and absence of organic substrates [43, 67]. Reaction of nitric oxide with Fe^{II} generates an EPR-active iron-nitrosyl complex that is a sensitive probe of organic substrate-induced changes to the active site. In the absence of organic substrate, the nitrosyl complex exhibits an axial EPR signal with g values at ~4 and ~2 consistent with an S=3/2 electronic configuration. In the presence of organic substrate, the Fe-NO complex becomes less symmetric as evidenced by the near quantitative formation of two new rhombic species with E/D values of ~ 0.024 and ~ 0.12. Under the assumption that the mode of NO binding to the iron center is similar to that of O_2, these EPR results indicate the O_2 binds in close proximity to the organic substrate, with the most

likely coordination site being *trans* to the first conserved His residue (His197 in CAO1). This placement is consistent with the proposed site of O_2 binding in both ACO and VP14 as described earlier.

Notably, the Fe^{II} centers of stilbene-cleaving CCDs, like that of ACO, quantitatively react with nitric oxide in the absence of organic substrate – a finding that has been used to argue against a role for organic substrate in gating the binding of O_2 [67]. However, the affinity of non-heme Fe^{II} centers for NO is typically higher than for O_2, so that NO binding results might not be extrapolated to O_2. In fact, ^{57}Fe-labeled samples of NOV2 exposed to ~ 3 atmospheres of pure O_2 exhibited Mössbauer spectra identical to anaerobic samples, indicating a very low affinity for the gas in the absence of organic substrate [43].

Surface features

Unlike typical CCDs, stilbene-cleaving members do not contain hydrophobic patches on their surfaces that could be used for insertion into membranes for substrate acquisition. This finding implies that the stilbene substrates are taken up from the aqueous environment although stilbenes like resveratrol are moderately hydrophobic and are known to partition into lipid bilayers. Most of the residues in CAO1 that align with residues comprising the non-polar patch of ACO are polar or charged. The few remaining equivalent hydrophobic side chains are buried in the protein interior and are partially responsible for sealing off the hydrophobic substrate entry tunnel found in ACO and other CCDs [43]. Besides these hydrophobic residues, a number of charged side chains also protrude into the potential cavity resulting in the complete absence of a passageway in this region of these enzymes.

Oligomeric structure

All stilbene-cleaving CCD crystal structures determined to date exhibit a conserved 2-fold dimeric assembly. The dimer interface is comprised of an antiparallel β-strand interaction formed by residues of the outer β-strand of blade VII together with polar and nonpolar interactions involving residues within the *N*-terminal segments of the proteins along with various other residues depending on the particular structure. Interactions mediating the dimer interface have been described in detail for CAO1 [43] and LsdA [69]. The dimeric structure buries ~1400-1500 Å in all of the structures except in NOV1 where the interface is smaller (~930 $Å^2$). Δ^iG values calculated with PISA [73] indicate the dimers have variable stability in solution with PbLSD and CAO1 having the greatest and least hydrophobic interfaces, respectively. However, in all cases the dimeric assembly in not predicted to be exceptionally stable and it is likely that subunits could readily exchange in solution. Dimerization of LSD enzymes is well documented in the literature [74, 75] and CAO1 also appears to be dimeric in solution based on size exclusion chromatography results [43]. However, PbLSD was reported to behave as a monomer in solution [68]. The conserved interface strongly suggests that dimerization occurs *in vivo* although the physiological relevance of the dimeric structure is obscure.

Mechanistic studies

The stilbene-cleaving CCDs represent the mechanistically best characterized subfamily of CCDs owing to their robust heterologous expression, reasonable aqueous solubility of their

stilbenoid substrates, and the availability of high resolution structures of substrate and product complexes on which to base high-level computational studies.

Isotope labeling studies have been used to determine the stoichiometry of O_2 incorporation during cleavage as well as the influence of deuterium substitution on steady-state kinetics. Initial O_2-labeling studies on NOV2, a paralog of NOV1 with largely similar substrate specificity, indicated that this protein operated as a monooxygenase [62]. However, these studies employed crude *E. coli* cell lysates with the extraneous proteins contributing to oxygen back-exchange, a problem that has complicated determination of the reaction stoichiometry. This issue was later revisited using purified protein and optimized reaction conditions with results clearly supporting dioxygenase chemistry [43]. More recently, solvent kinetic isotope effect (sKIE) studies have been carried out on NOV2 and CAO1 to determine the impact of deuterium substitution on steady-state kinetics [76]. These studies revealed a striking difference in behavior with NOV2 and CAO1 exhibiting inverse and normal sKIEs on k_{cat}, respectively. The inverse sKIE displayed by NOV2 was rationalized as iron-aquo dissociation being involved in a rate-limiting step in the NOV2 catalytic cycle, which is known to be thermodynamically more favorable when deuterium is substituted for hydrogen in the solvent. The normal sKIE observed for CAO1 was suggestive of proton transfer during the rate-limiting step of the reaction, although the exact proton source could not be pinpointed. Interestingly, inverse sKIE behavior could be conferred to CAO1 by substitution of a single amino acid residue (Leu509) located near the iron-solvent compex to Val as is found in NOV2 [76].

Computational studies

The reaction mechanism of stilbene-cleaving CCDs has been examined by two independent quantum mechanics/molecular mechanics studies using the NOV1-resveratrol-O_2 complex derived from crystallography [67] as a starting model. These studies differ in several details but both conclude that the reaction proceeds through a dioxetane intermediate that collapses to generate the two aldehyde products both containing oxygen derived from O_2. The studies are thus consistent with stilbene-cleaving CCDs acting as dioxygenases (Fig. 9). In the study by Bai et al, the initial reactive species was identified as an end-on Fe^{III}-O_2^- complex with a triplet or quintet spin state [77]. The lowest energy barrier reaction pathway involved attack of the activated oxygen on the α-carbon of resveratrol to generate a resonance-stabilized free radical involving the 4’-hydroxyl group. Following an isomerization of the peroxo bridge, a dioxetane intermediate is formed through reaction of the iron-bound oxygen atom with the β-carbon. Rupture of the dioxetane O-O bond is then kinetically facile and may be promoted by interaction with the iron cofactor. This is followed by cleavage of the α,β-carbon bond to form the aldehyde products. The protonation states of Lys134 and 4’-hydroxyl minimally affected the transition state energies suggesting that the interaction between these two groups is strictly for proper substrate positioning rather than to enable proton shuttling. The study by Lu, *et al.* found the initial reactive state to be a side-on Fe^{II}-O_2^- complex with partial electron transfer from resveratrol to the iron-oxy complex [78]. For the quintet spin state, the unpaired electrons on O_2 and resveratrol have anti-parallel spins suitable for peroxo bridge formation between O_2 and the α-carbon of resveratrol. Attack of O1 on the β-carbon of resveratrol forms a dioxetane structure that decomposes into the aldehyde products

in a manner similar to that described in the previous study. In both studies, the attack of activated oxygen on the α-carbon on the stilbene substrate reaction was identified as rate-limiting on the quintet surface and the cleavage reaction was found to be highly exergonic as expected. Neither of these studies investigated the strength of oxygen binding to the iron center in the absence of substrate. However, the initial electron transfer from the stilbene to the iron-oxy complex identified in the latter study is similar to what was found for the mechanism of ACO catalysis [46] and could provide a mechanism whereby O_2 binding and activation only occurs in the presence of organic substrate. Two important limitations of these studies are their reliance on a starting model that has questionable experimental support [71] and omission of the conserved Thr residue located near the iron cofactor *trans* to His284 which most likely influences O_2 binding orientation through steric effects. Notwithstanding these criticisms, both studies provided important theoretical insights forming a basis for further experimental studies on the reaction mechanism of stilbene-cleaving CCDs.

Metazoan CCDs

Introduction

Although the central cleavage of beta carotene was known since the 1950's to be mediated by an enzymatic activity it wasn't until early 2000's that the first carotenoid-cleaving metazoan CCDs were cloned. The first of these was the "neither inactivation nor afterpotential B" (NinaB) gene from *Drosophila* [7, 79] and beta carotene oxygenase 1 (BCO1) from *Gallus gallus* [4]. These efforts were followed by the cloning of 15,15'-β-carotene oxygenases from various vertebrate species [5, 6, 8] as well as the cloning of a second carotene oxygenase catalyzing the eccentric 9-10 (9'-10') cleavage of β-carotenoids, known as BCO2 [10]. The identification of these two types of enzymes helped resolve a long-standing controversy that revolved around whether formation of retinal from provitamin A carotenoids was achieved through central or excentric cleavage [80, 81]. In fact, both processes are now known to contribute to vitamin A generation in mammals [82, 83].

While substantial progress has been made in understanding the substrate specificity and biochemical properties of vertebrate BCO1 and BCO2 as well as insect NinaB proteins, no high resolution structures of these enzymes have been reported to date. BCO1 and BCO2 are closely related to a third CCD superfamily member present in vertebrates known as RPE65, which functions as a retinoid isomerohydrolase rather than a carotenoid cleaving enzyme [84]. Phylogenetically, this enzyme is most closely related to BCO2 proteins and the enzymes share ~40% sequence identity (Figs. 1A and 10). Hence, the known three-dimensional structure of RPE65 provides a suitable template for modeling of BCO2 as previously described [83]. Below, we describe structural features of BCO2 that have been inferred from a homology model generated from the bovine RPE65 crystal structure [85] (Fig. 11). This is followed by a discussion of mechanistic studies carried out on NinaB proteins to elucidate the basis of their substrate specificity as well as double bond isomerization activity.

BCO2 sequence features

Vertebrate BCO2 amino acid sequences are typically around ~570 amino acids in length. In comparison to BCO1 and RPE65 proteins, most BCO2 sequences feature an *N*-terminal extension that functions as a mitochondrial localization sequence [86, 87]. Interestingly, this leader sequence is not essential for mitochondrial targeting as the mouse BCO2 sequence lacks the extension but nevertheless localizes to the inner mitochondrial membrane. BCO2 proteins also feature other sequence elements that are characteristic of metazoan and/or vertebrate CCD enzymes. These include a PDPCK sequence [88] located in a loop connecting beta sheets 1 and 2 that is likely involved in mediating membrane interactions as discussed below. Primate sequences contain a 4 amino acid insertion on the C-terminal end of this loop that has been proposed to inactivate BCO2 leading to the accumulation of carotenoids in the macular region of the eye [89] although other studies have failed to confirm this idea [90]. BCO2 sequences also contain a vertebrate-specific ~30 amino-acid insertion at the *C*-terminus of blade 4 that is similar in length and sequence to a corresponding insertion found in RPE65 that mediates formation of a homodimeric assembly. This two-fold symmetric dimer structure has been repeatedly observed *in crystallo* and is likely physiologically relevant [91].

Metal center.

The predicted metal center of BCO2 is reminiscent of other CCDs with a 4-His primary coordination sphere and three second sphere Glu residues (Fig. 11). The sixth coordination is probably occluded by a nearby Val residue, like that observed for RPE65 and similar to the sixth-site occlusion by Thr in ACO and the stilbene-cleaving CCDs.

Membrane binding:

Alignment of BCO2 with RPE65 (Fig. 10) reveals that residues predicted to mediate membrane interactions are relatively well conserved between these two groups of proteins. This includes the sequence downstream of the metazoan-specific PDPCK motif (residues 108-125 in mouse BCO2), which is disordered in RPE65 crystal structures but has been predicted to adopt an amphipathic alpha-helix conformation under some conditions [85, 92]. The other three regions consist of either hydrophobic or positively charged residues both of which could promote interaction of the protein with inner mitochondrial membranes where the protein is localized *in vivo*. However, like other CCDs with membrane-binding patches [93, 94], BCO2 can behave to some extent like a soluble protein when heterologously expressed [95].

Active site determinants of substrate specificity:

Besides the difference in cleavage regioselectivity that differentiates BCO2 from BCO1, these enzymes also have fundamentally different substrate specificities. BCO2 has a preference for xanthophyll and hydroxylated apocarotenoid substrates [90, 95] as well as various isomers of lycopene [10, 96] whereas BCO1 prefers carotenoid and apocarotenoid substrates with at least one unsubstituted beta-ionone ring and has weaker activity towards lycopene [5, 83, 95, 97, 98]. The active site determinants of this differing substrate specificity have been examined through mutagenesis studies of residues located close to the

opening of the active site tunnel. In particular, sequence alignments between human BCO1 and mouse BCO2 revealed a difference at two relevant positions in the sequence alignment: Trp270 (paralogous to Phe272 in mBCO2) and Leu168 (paralogous to Gly175 in mBCO2). Mutagenesis to transfer the BCO2-associated residues at these positions to those in BCO1 conferred an ability to cleave the xanthophyll, zeaxanthin, not exhibited by the native BCO1 protein [83]. In another study, it was discovered that P108S and N190D polymorphisms in the mouse BCO2 sequence boost catalytic activity towards lycopene [88]. Notably the residues examined in both studies all localize at or near the predicted substrate entry tunnel, thus confirming the key role of this region in governing substrate specificity.

Mechanistic studies on insect NinaB proteins

Following the identification of NinaB as the first metazoan carotenoid cleaving enzyme, it was discovered that this protein also possesses the capability to *trans-cis* isomerize the 11-12 double bond of its substrate during the 15-15' oxidative cleavage reaction, thus behaving as an isomerooxygenase [15]. This property bears some resemblance to the isomerase activity of vertebrate RPE65, although RPE65 operates as an isomerohydrolase and is not known to cleave double bonds. The isomerase activity of NinaB was found to be part of an insect visual cycle that allows formation of visual pigments in dark conditions. This pathway is complementary to pigment regeneration via photoreversion, which is possible due to the bistable nature of insect visual pigments [99]. The active site determinants of this activity have been investigated by homology modeling, targeted mutagenesis, and substrate specificity studies [100]. Specifically, it was found that *trans-cis* isomerization preferentially occurs at the 11-12 double bond closest to the 3-hydroxy-β-ionone ring of the substrate, which ensures production of biologically active chromophore. Mutagenesis studies revealed that aromatic residues in the active site cavity play a pivotal role in catalysis possibly by stabilizing a putative substrate free radical generated during catalysis [100]. NinaB was also confirmed to catalyze a dioxygenase-based cleavage reaction [100].

Conclusions and Future Directions

Our understanding of catalysis by CCDs has advanced dramatically over the past decade as a result of improvements in expression protocols for these enzymes, innovative biochemical and biophysical investigations, and determination of crystal structures from diverse subfamilies of these enzymes. As a result of these studies, we now are beginning to understand the common and divergent properties of the CCD superfamily. Multiple studies have confirmed that the CCDs from diverse subfamilies are in fact dioxygenases, which was previously a major point of contention. Computational studies also indicate that attack of O_2 on the alkene substrate may be a rate-limiting step common to the entire family. Additionally, the iron centers of these proteins are remarkably well-conserved even among RPE65 proteins, which have undergone catalytic neofunctionalization. By contrast, it is now clear that the loops and helices forming the substrate-binding clefts of CCDs have a huge capacity for structural changes to enable the binding of diverse substrates. Despite these notable accomplishments, there is still much work left to do in this field to fully elucidate the mechanistic basis of CCD activity.

For example, the lack of genuine CCD-carotenoid complex structures has precluded a detailed understanding of the active site determinants of substrate specificity. From the preceding sections, it is clear that such determinants are likely variable for the different subfamilies of CCDs according to their particular substrate specificities. However, given the known difficulty in obtaining such complexes as a result of the extreme hydrophobicity of most carotenoids, innovative strategies including use of water soluble carotenoids or specialized crystallization conditions will likely be required. Further structural studies will also likely be of key importance in resolving the mechanisms of CCDs with secondary catalytic properties such as CCD8 and NinaB as described earlier.

A second area where uncertainty still exists is in understanding the specific intermediates that are formed during CCD catalysis. Although quantum chemical studies have suggested reactive iron-oxygen species that could plausibly be involved in the oxidative cleavage reaction, it is important to note that these studies have not been calibrated by any spectroscopically defined reaction intermediates. Methods that have been developed to generate ^{57}Fe-labeled and metal-substituted CCDs should help facilitate advanced physical studies such as rapid freeze-quench Mössbauer spectroscopy that can reveal the electronic state of iron in reaction intermediates. Additionally, hypotheses generated regarding carotenoid intermediates could be fruitfully tested with putative transition states analogs as has been described for RPE65 [101]. As CCD inhibition may be beneficial for certain agricultural and medical purposes, the development of such compounds may also have important practical utility.

With such important questions remaining to be fully addressed, we can look forward to another exciting decade of research on the structure and mechanism of carotenoid oxygenases.

Acknowledgements

This work was supported by grants from the Department of Veterans Affairs (IK2BX002683 to P.D.K), the National Institutes of Health (EY009339 to P.D.K) and institutional funds from the University of California Irvine. We apologize to authors whose work could not be included in this review owing to space limitations.

Abbreviations

ACO	*Synechocystis* apocarotenoid-15,15’-oxygenase
BCO	beta-carotene oxygenase
CAO1	Neurospora crassa oxygenase 1
CCD	carotenoid cleavage dioxygenase
EPR	electron paramagnetic resonance
LSD	lignostilbene dioxygenase
NCED	9-*cis*-epoxycarotenoid dioxygenase
NinaB	neither inactivation nor afterpotential B

NOV	*Novosphingobium aromaticavorans* oxygenase
RPE65	retinal pigment epithelium-specific 65 kDa protein
sKIE	solvent kinetic isotope effect
VP14	viviparous-14
XAS	X-ray absorption spectroscopy

References

[1]. Moore T, Vitamin A and carotene: The association of vitamin A activity with carotene in the carrot root, Biochem. J, 23 (1929) 803–811. [PubMed: 16744266]

[2]. Olson JA, Hayaishi O, The enzymatic cleavage of beta-carotene into vitamin A by soluble enzymes of rat liver and intestine, Proc. Natl. Acad. Sci. U.S.A, 54 (1965) 1364–1370. [PubMed: 4956142]

[3]. Goodman DS, Huang HS, Biosynthesis of Vitamin a with Rat Intestinal Enzymes, Science, 149 (1965) 879–880. [PubMed: 14332853]

[4]. Wyss A, Wirtz G, Woggon W, Brugger R, Wyss M, Friedlein A, Bachmann H, Hunziker W, Cloning and expression of beta,beta-carotene 15,15'-dioxygenase, Biochem. Biophys. Res. Commun, 271 (2000) 334–336. [PubMed: 10799297]

[5]. Redmond TM, Gentleman S, Duncan T, Yu S, Wiggert B, Gantt E, Cunningham FX Jr., Identification, expression, and substrate specificity of a mammalian beta-carotene 15,15'-dioxygenase, J. Biol. Chem, 276 (2001) 6560–6565. [PubMed: 11092891]

[6]. Paik J, During A, Harrison EH, Mendelsohn CL, Lai K, Blaner WS, Expression and characterization of a murine enzyme able to cleave beta-carotene. The formation of retinoids, J. Biol. Chem, 276 (2001) 32160–32168. [PubMed: 11418584]

[7]. von Lintig J, Vogt K, Filling the gap in vitamin A research. Molecular identification of an enzyme cleaving beta-carotene to retinal, J. Biol. Chem, 275 (2000) 11915–11920. [PubMed: 10766819]

[8]. Yan W, Jang GF, Haeseleer F, Esumi N, Chang J, Kerrigan M, Campochiaro M, Campochiaro P, Palczewski K, Zack DJ, Cloning and characterization of a human beta,beta-carotene-15,15'-dioxygenase that is highly expressed in the retinal pigment epithelium, Genomics, 72 (2001) 193–202. [PubMed: 11401432]

[9]. Schwartz SH, Tan BC, Gage DA, Zeevaart JA, McCarty DR, Specific oxidative cleavage of carotenoids by VP14 of maize, Science, 276 (1997) 1872–1874. [PubMed: 9188535]

[10]. Kiefer C, Hessel S, Lampert JM, Vogt K, Lederer MO, Breithaupt DE, von Lintig J, Identification and characterization of a mammalian enzyme catalyzing the asymmetric oxidative cleavage of provitamin A, J. Biol. Chem, 276 (2001) 14110–14116. [PubMed: 11278918]

[11]. Kamoda S, Saburi Y, Cloning, expression, and sequence analysis of a lignostilbene-alpha,beta-dioxygenase gene from Pseudomonas paucimobilis TMY1009, Biosci. Biotechnol. Biochem, 57 (1993) 926–930. [PubMed: 7763879]

[12]. Tan BC, Schwartz SH, Zeevaart JA, McCarty DR, Genetic control of abscisic acid biosynthesis in maize, Proc. Natl. Acad. Sci. U.S.A, 94 (1997) 12235–12240. [PubMed: 9342392]

[13]. Huang FC, Horvath G, Molnar P, Turcsi E, Deli J, Schrader J, Sandmann G, Schmidt H, Schwab W, Substrate promiscuity of RdCCD1, a carotenoid cleavage oxygenase from Rosa damascena, Phytochemistry, 70 (2009) 457–464. [PubMed: 19264332]

[14]. Frusciante S, Diretto G, Bruno M, Ferrante P, Pietrella M, Prado-Cabrero A, Rubio-Moraga A, Beyer P, Gomez-Gomez L, Al-Babili S, Giuliano G, Novel carotenoid cleavage dioxygenase catalyzes the first dedicated step in saffron crocin biosynthesis, Proc. Natl. Acad. Sci. U.S.A, 111 (2014) 12246–12251. [PubMed: 25097262]

[15]. Oberhauser V, Voolstra O, Bangert A, von Lintig J, Vogt K, NinaB combines carotenoid oxygenase and retinoid isomerase activity in a single polypeptide, Proc. Natl. Acad. Sci. U.S.A, 105 (2008) 19000–19005. [PubMed: 19020100]

[16]. Alder A, Jamil M, Marzorati M, Bruno M, Vermathen M, Bigler P, Ghisla S, Bouwmeester H, Beyer P, Al-Babili S, The path from beta-carotene to carlactone, a strigolactone-like plant hormone, Science, 335 (2012) 1348–1351. [PubMed: 22422982]

[17]. Redmond TM, Poliakov E, Yu S, Tsai JY, Lu Z, Gentleman S, Mutation of key residues of RPE65 abolishes its enzymatic role as isomerohydrolase in the visual cycle, Proc. Natl. Acad. Sci. U.S.A, 102 (2005) 13658–13663. [PubMed: 16150724]

[18]. Moiseyev G, Chen Y, Takahashi Y, Wu BX, Ma JX, RPE65 is the isomerohydrolase in the retinoid visual cycle, Proc. Natl. Acad. Sci. U.S.A, 102 (2005) 12413–12418. [PubMed: 16116091]

[19]. Kloer DP, Ruch S, Al-Babili S, Beyer P, Schulz GE, The structure of a retinal-forming carotenoid oxygenase, Science, 308 (2005) 267–269. [PubMed: 15821095]

[20]. Dellus-Gur E, Toth-Petroczy A, Elias M, Tawfik DS, What Makes a Protein Fold Amenable to Functional Innovation? Fold Polarity and Stability Trade-offs, J. Mol. Biol, 425 (2013) 2609–2621. [PubMed: 23542341]

[21]. Pandya C, Farelli JD, Dunaway-Mariano D, Allen KN, Enzyme Promiscuity: Engine of Evolutionary Innovation, J. Biol. Chem, 289 (2014) 30229–30236. [PubMed: 25210039]

[22]. Hegg EL, Que L Jr., The 2-His-1-carboxylate facial triad--an emerging structural motif in mononuclear non-heme iron(II) enzymes, Eur. J. Biochem, 250 (1997) 625–629. [PubMed: 9461283]

[23]. Liang MH, Zhu J, Jiang JG, Carotenoids biosynthesis and cleavage related genes from bacteria to plants, Crit. Rev. Food Sci. Nutr, 58 (2018) 2314–2333. [PubMed: 28609133]

[24]. Walter MH, Strack D, Carotenoids and their cleavage products: Biosynthesis and functions, Nat. Prod. Rep, 28 (2011) 663–692. [PubMed: 21321752]

[25]. Auldridge ME, McCarty DR, Klee HJ, Plant carotenoid cleavage oxygenases and their apocarotenoid products, Curr. Opin. Plant Biol, 9 (2006) 315–321. [PubMed: 16616608]

[26]. Al-Babili S, Bouwmeester HJ, Strigolactones, a novel carotenoid-derived plant hormone, Annu. Rev. Plant Biol, 66 (2015) 161–186. [PubMed: 25621512]

[27]. Harrison EH, Quadro L, Apocarotenoids: Emerging Roles in Mammals, Annu. Rev. Nutr, 38 (2018) 153–172. [PubMed: 29751734]

[28]. Ahrazem O, Gomez-Gomez L, Rodrigo MJ, Avalos J, Limon MC, Carotenoid Cleavage Oxygenases from Microbes and Photosynthetic Organisms: Features and Functions, Int. J. Mol. Sci, 17 (2016).

[29]. von Lintig J, Colors with functions: elucidating the biochemical and molecular basis of carotenoid metabolism, Annu. Rev. Nutr, 30 (2010) 35–56. [PubMed: 20415581]

[30]. Sui X, Kiser PD, Lintig J, Palczewski K, Structural basis of carotenoid cleavage: from bacteria to mammals, Arch. Biochem. Biophys, 539 (2013) 203–213. [PubMed: 23827316]

[31]. Harrison PJ, Bugg TD, Enzymology of the carotenoid cleavage dioxygenases: reaction mechanisms, inhibition and biochemical roles, Arch. Biochem. Biophys, 544 (2014) 105–111. [PubMed: 24144525]

[32]. Kloer DP, Schulz GE, Structural and biological aspects of carotenoid cleavage, Cell. Mol. Life Sci, 63 (2006) 2291–2303. [PubMed: 16909205]

[33]. Kiser PD, Alkene-cleaving carotenoid cleavage dioxygenases, in: Scott RA (Ed.) Encyclopedia of Inorganic and Bioinorganic Chemistry, John Wiley & Sons, Ltd, 2019. doi: 10.1002/9781119951438.eibc2702

[34]. Juttner F, Hoflacher B, Evidence of Beta-Carotene 7,8 (7',8') Oxygenase (Beta-Cyclocitral, Crocetindial Generating) in Microcystis, Arch. Microbiol, 141 (1985) 337–343.

[35]. Ruch S, Beyer P, Ernst H, Al-Babili S, Retinal biosynthesis in Eubacteria: in vitro characterization of a novel carotenoid oxygenase from Synechocystis sp. PCC 6803, Mol. Microbiol, 55 (2005) 1015–1024. [PubMed: 15686550]

[36]. Chen Q, van der Steen JB, Arents JC, Hartog AF, Ganapathy S, de Grip WJ, Hellingwerf KJ, Deletion of sll1541 in Synechocystis sp. Strain PCC 6803 Allows Formation of a Far-Red-Shifted holo-Proteorhodopsin In Vivo, Appl. Environ. Microbiol, 84 (2018).

[37]. Marasco EK, Vay K, Schmidt-Dannert C, Identification of carotenoid cleavage dioxygenases from Nostoc sp. PCC 7120 with different cleavage activities, J. Biol. Chem, 281 (2006) 31583–31593. [PubMed: 16920703]

[38]. Heo J, Kim SH, Lee PC, New insight into the cleavage reaction of Nostoc sp. strain PCC 7120 carotenoid cleavage dioxygenase in natural and nonnatural carotenoids, Appl. Environ. Microbiol, 79 (2013)3336–3345. [PubMed: 23524669]

[39]. Scherzinger D, Ruch S, Kloer DP, Wilde A, Al-Babili S, Retinal is formed from apo-carotenoids in Nostoc sp. PCC7120: in vitro characterization of an apo-carotenoid oxygenase, Biochem. J, 398 (2006) 361–369. [PubMed: 16759173]

[40]. Britton G, Structure and properties of carotenoids in relation to function, FASEB J, 9 (1995) 1551–1558. [PubMed: 8529834]

[41]. Sui X, Kiser PD, Che T, Carey PR, Golczak M, Shi W, von Lintig J, Palczewski K, Analysis of carotenoid isomerase activity in a prototypical carotenoid cleavage enzyme, apocarotenoid oxygenase (ACO), J. Biol. Chem, 289 (2014) 12286–12299. [PubMed: 24648526]

[42]. Sui X, Golczak M, Zhang J, Kleinberg KA, von Lintig J, Palczewski K, Kiser PD, Utilization of Dioxygen by Carotenoid Cleavage Oxygenases, J. Biol. Chem, 290 (2015) 30212–30223. [PubMed: 26499794]

[43]. Sui X, Weitz AC, Farquhar ER, Badiee M, Banerjee S, von Lintig J, Tochtrop GP, Palczewski K, Hendrich MP, Kiser PD, Structure and Spectroscopy of Alkene-Cleaving Dioxygenases Containing an Atypically Coordinated Non-Heme Iron Center, Biochemistry, 56 (2017) 2836–2852. [PubMed: 28493664]

[44]. Sui X, Zhang J, Golczak M, Palczewski K, Kiser PD, Key Residues for Catalytic Function and Metal Coordination in a Carotenoid Cleavage Dioxygenase, J. Biol. Chem, 291 (2016) 19401–19412. [PubMed: 27453555]

[45]. Sui X, Farquhar ER, Hill HE, von Lintig J, Shi W, Kiser PD, Preparation and characterization of metal-substituted carotenoid cleavage oxygenases, J. Biol. Inorg. Chem, 23 (2018) 887–901. [PubMed: 29946976]

[46]. Borowski T, Blomberg MR, Siegbahn PE, Reaction mechanism of apocarotenoid oxygenase (ACO): a DFT study, Chemistry, 14 (2008) 2264–2276. [PubMed: 18181127]

[47]. Vogel JT, Tan BC, McCarty DR, Klee HJ, The carotenoid cleavage dioxygenase 1 enzyme has broad substrate specificity, cleaving multiple carotenoids at two different bond positions, J. Biol. Chem, 283 (2008) 11364–11373. [PubMed: 18285342]

[48]. Ilg A, Bruno M, Beyer P, Al-Babili S, Tomato carotenoid cleavage dioxygenases 1A and 1B: Relaxed double bond specificity leads to a plenitude of dialdehydes, mono-apocarotenoids and isoprenoid volatiles, FEBS Open Bio., 4 (2014) 584–593.

[49]. Ohmiya A, Kishimoto S, Aida R, Yoshioka S, Sumitomo K, Carotenoid cleavage dioxygenase (CmCCD4a) contributes to white color formation in chrysanthemum petals, Plant Physiol., 142 (2006) 1193–1201. [PubMed: 16980560]

[50]. Zhang B, Liu C, Wang Y, Yao X, Wang F, Wu J, King GJ, Liu K, Disruption of a CAROTENOID CLEAVAGE DIOXYGENASE 4 gene converts flower colour from white to yellow in Brassica species, New Phytol., 206 (2015) 1513–1526. [PubMed: 25690717]

[51]. Campbell R, Ducreux LJ, Morris WL, Morris JA, Suttle JC, Ramsay G, Bryan GJ, Hedley PE, Taylor MA, The metabolic and developmental roles of carotenoid cleavage dioxygenase4 from potato, Plant Physiol., 154 (2010) 656–664. [PubMed: 20688977]

[52]. Rodrigo MJ, Alquezar B, Alos E, Medina V, Carmona L, Bruno M, Al-Babili S, Zacarias L, A novel carotenoid cleavage activity involved in the biosynthesis of Citrus fruit-specific apocarotenoid pigments, J. Exp. Bot, 64 (2013) 4461–4478. [PubMed: 24006419]

[53]. Messing SA, Gabelli SB, Echeverria I, Vogel JT, Guan JC, Tan BC, Klee HJ, McCarty DR, Amzel LM, Structural insights into maize viviparous14, a key enzyme in the biosynthesis of the phytohormone abscisic acid, Plant Cell, 22 (2010) 2970–2980. [PubMed: 20884803]

[54]. Tan BC, Cline K, McCarty DR, Localization and targeting of the VP14 epoxy-carotenoid dioxygenase to chloroplast membranes, Plant J., 27 (2001) 373–382. [PubMed: 11576422]

[55]. Costas M, Mehn MP, Jensen MP, Que L Jr., Dioxygen activation at mononuclear nonheme iron active sites: enzymes, models, and intermediates, Chem. Rev, 104 (2004) 939–986. [PubMed: 14871146]

[56]. Schwartz SH, Tan BC, McCarty DR, Welch W, Zeevaart JA, Substrate specificity and kinetics for VP14, a carotenoid cleavage dioxygenase in the ABA biosynthetic pathway, Biochim. Biophys. Acta, 1619 (2003) 9–14. [PubMed: 12495810]

[57]. Auldridge ME, Block A, Vogel JT, Dabney-Smith C, Mila I, Bouzayen M, Magallanes-Lundback M, DellaPenna D, McCarty DR, Klee HJ, Characterization of three members of the Arabidopsis carotenoid cleavage dioxygenase family demonstrates the divergent roles of this multifunctional enzyme family, Plant J., 45 (2006) 982–993. [PubMed: 16507088]

[58]. Schwartz SH, Qin X, Zeevaart JA, Characterization of a novel carotenoid cleavage dioxygenase from plants, J. Biol. Chem, 276 (2001) 25208–25211. [PubMed: 11316814]

[59]. Schmidt H, Kurtzer R, Eisenreich W, Schwab W, The carotenase AtCCD1 from Arabidopsis thaliana is a dioxygenase, J. Biol. Chem, 281 (2006) 9845–9851. [PubMed: 16459333]

[60]. Bruno M, Vermathen M, Alder A, Wust F, Schaub P, van der Steen R, Beyer P, Ghisla S, Al-Babili S, Insights into the formation of carlactone from in-depth analysis of the CCD8-catalyzed reactions, FEBS Lett., 591 (2017) 792–800. [PubMed: 28186640]

[61]. Harrison PJ, Newgas SA, Descombes F, Shepherd SA, Thompson AJ, Bugg TD, Biochemical characterization and selective inhibition of beta-carotene cis-trans isomerase D27 and carotenoid cleavage dioxygenase CCD8 on the strigolactone biosynthetic pathway, FEBS J., 282 (2015) 3986–4000. [PubMed: 26257333]

[62]. Marasco EK, Schmidt-Dannert C, Identification of bacterial carotenoid cleavage dioxygenase homologues that cleave the interphenyl alpha,beta double bond of stilbene derivatives via a monooxygenase reaction, Chembiochem, 9 (2008) 1450–1461. [PubMed: 18478524]

[63]. Diaz-Sanchez V, Estrada AF, Limon MC, Al-Babili S, Avalos J, The oxygenase CAO-1 of Neurospora crassa is a resveratrol cleavage enzyme, Eukaryot. Cell, 12 (2013) 1305–1314. [PubMed: 23893079]

[64]. Brefort T, Scherzinger D, Limon MC, Estrada AF, Trautmann D, Mengel C, Avalos J, Al-Babili S, Cleavage of resveratrol in fungi: characterization of the enzyme Rco1 from Ustilago maydis, Fungal Genet. Biol, 48 (2011) 132–143. [PubMed: 21073977]

[65]. Yu RQ, Kurt Z, He F, Spain JC, Biodegradation of the Allelopathic Chemical Pterostilbene by a Sphingobium sp. Strain from the Peanut Rhizosphere, Appl. Environ. Microbiol, 85 (2019).

[66]. Kurt Z, Minoia M, Spain JC, Resveratrol as a Growth Substrate for Bacteria from the Rhizosphere, Appl. Environ. Microbiol, 84 (2018).

[67]. McAndrew RP, Sathitsuksanoh N, Mbughuni MM, Heins RA, Pereira JH, George A, Sale KL, Fox BG, Simmons BA, Adams PD, Structure and mechanism of NOV1, a resveratrol-cleaving dioxygenase, Proc. Natl. Acad. Sci. U.S.A, 113 (2016) 14324–14329. [PubMed: 27911781]

[68]. Loewen PC, Switala J, Wells JP, Huang F, Zara AT, Allingham JS, Loewen MC, Structure and function of a lignostilbene-alpha,beta-dioxygenase orthologue from Pseudomonas brassicacearum, BMC Biochem, 19 (2018) 8. [PubMed: 30115012]

[69]. Kuatsjah E, Verstraete MM, Kobylarz MJ, Liu AKN, Murphy MEP, Eltis LD, Identification of functionally important residues and structural features in a bacterial lignostilbene dioxygenase, J. Biol. Chem, 294 (2019) 12911–12920. [PubMed: 31292192]

[70]. Holm L, Laakso LM, Dali server update, Nucleic Acids Res, 44 (2016) W351–355. [PubMed: 27131377]

[71]. Kiser PD, Reappraisal of dioxygen binding in NOV1 crystal structures, Proc. Natl. Acad. Sci. U.S.A, 114 (2017) E6027–E6028. [PubMed: 28679636]

[72]. Kamoda S, Terada T, Saburi Y, A common structure of substrate shared by lignostilbenedioxygenase isozymes from Sphingomonas paucimobilis TMY1009, Biosci. Biotechnol. Biochem, 67 (2003) 1394–1396. [PubMed: 12843670]

[73]. Krissinel E, Henrick K, Inference of macromolecular assemblies from crystalline state, J. Mol. Biol, 372 (2007) 774–797. [PubMed: 17681537]

[74]. Kamoda S, Terada T, Saburi Y, Production of heterogeneous dimer lignostilbenedioxygenase II from lsdA and lsdB in Escherichia coli cells, Biosci. Biotechnol. Biochem, 69 (2005) 635–637. [PubMed: 15784996]

[75]. Kamoda S, Saburi Y, Structural and enzymatical comparison of lignostilbene-alpha,beta-dioxygenase isozymes, I, II, and III, from Pseudomonas paucimobilis TMY1009, Biosci. Biotechnol. Biochem, 57 (1993) 931–934. [PubMed: 7763880]

[76]. Khadka N, Farquhar ER, Hill HE, Shi W, von Lintig J, Kiser PD, Evidence for distinct rate-limiting steps in the cleavage of alkenes by carotenoid cleavage dioxygenases, J. Biol. Chem, 294 (2019) 10596–10606. [PubMed: 31138651]

[77]. Bai J, Hou QQ, Zhu WY, Liu YJ, Mechanical insights into the oxidative cleavage of resveratrol catalyzed by dioxygenase NOV1 from Novosphingobium aromaticivorans: confirmation of dioxygenase mechanism by QM/MM calculations, Catal. Sci. Technol, 9 (2019) 444–455.

[78]. Lu J, Lai W, Mechanistic Insights into a Stibene Cleavage Oxygenase NOV1 from Quantum Mechanical/Molecular Mechanical Calculations, ChemistryOpen, 8 (2019) 228–235. [PubMed: 30828510]

[79]. von Lintig J, Dreher A, Kiefer C, Wernet MF, Vogt K, Analysis of the blind Drosophila mutant ninaB identifies the gene encoding the key enzyme for vitamin A formation invivo, Proc. Natl. Acad. Sci. U.S.A, 98 (2001) 1130–1135. [PubMed: 11158606]

[80]. Wolf G, The enzymatic cleavage of beta-carotene: end of a controversy, Nutr. Rev, 59 (2001) 116–118. [PubMed: 11368505]

[81]. Wolf G, The enzymatic cleavage of beta-carotene: still controversial, Nutr. Rev, 53 (1995) 134–137. [PubMed: 7666986]

[82]. Amengual J, Widjaja-Adhi MA, Rodriguez-Santiago S, Hessel S, Golczak M, Palczewski K, von Lintig J, Two carotenoid oxygenases contribute to mammalian provitamin A metabolism, J. Biol. Chem, 288 (2013) 34081–34096. [PubMed: 24106281]

[83]. Kelly ME, Ramkumar S, Sun W, Colon Ortiz C, Kiser PD, Golczak M, von Lintig J, The Biochemical Basis of Vitamin A Production from the Asymmetric Carotenoid beta-Cryptoxanthin, ACS Chem. Biol, 13 (2018) 2121–2129. [PubMed: 29883100]

[84]. Redmond TM, Yu S, Lee E, Bok D, Hamasaki D, Chen N, Goletz P, Ma JX, Crouch RK, Pfeifer K, Rpe65 is necessary for production of 11-cis-vitamin A in the retinal visual cycle, Nat. Genet, 20 (1998) 344–351. [PubMed: 9843205]

[85]. Kiser PD, Golczak M, Lodowski DT, Chance MR, Palczewski K, Crystal structure of native RPE65, the retinoid isomerase of the visual cycle, Proc. Natl. Acad. Sci. U.S.A, 106 (2009) 17325–17330. [PubMed: 19805034]

[86]. Palczewski G, Amengual J, Hoppel CL, von Lintig J, Evidence for compartmentalization of mammalian carotenoid metabolism, FASEB J., 28 (2014) 4457–4469. [PubMed: 25002123]

[87]. Amengual J, Lobo GP, Golczak M, Li HN, Klimova T, Hoppel CL, Wyss A, Palczewski K, von Lintig J, A mitochondrial enzyme degrades carotenoids and protects against oxidative stress, FASEB J., 25 (2011) 948–959. [PubMed: 21106934]

[88]. Poliakov E, Soucy J, Gentleman S, Rogozin IB, Redmond TM, Phylogenetic analysis of the metazoan carotenoid oxygenase superfamily: a new ancestral gene assemblage of BCO-like (BCOL) proteins, Sci. Rep, 7 (2017) 13192. [PubMed: 29038443]

[89]. Li B, Vachali PP, Gorusupudi A, Shen Z, Sharifzadeh H, Besch BM, Nelson K, Horvath MM, Frederick JM, Baehr W, Bernstein PS, Inactivity of human beta,beta-carotene-9',10'-dioxygenase (BCO2) underlies retinal accumulation of the human macular carotenoid pigment, Proc. Natl. Acad. Sci. U.S.A, 111 (2014) 10173–10178. [PubMed: 24982131]

[90]. Babino D, Palczewski G, Widjaja-Adhi MA, Kiser PD, Golczak M, von Lintig J, Characterization of the Role of beta-Carotene 9,10-Dioxygenase in Macular Pigment Metabolism, J. Biol. Chem, 290 (2015) 24844–24857. [PubMed: 26307071]

[91]. Kiser PD, Farquhar ER, Shi W, Sui X, Chance MR, Palczewski K, Structure of RPE65 isomerase in a lipidic matrix reveals roles for phospholipids and iron in catalysis, Proc. Natl. Acad. Sci. U.S.A, 109 (2012) E2747–2756. [PubMed: 23012475]

[92]. Hamel CP, Tsilou E, Pfeffer BA, Hooks JJ, Detrick B, Redmond TM, Molecular cloning and expression of RPE65, a novel retinal pigment epithelium-specific microsomal protein that is post-transcriptionally regulated in vitro, J. Biol. Chem, 268 (1993) 15751–15757. [PubMed: 8340400]

[93]. Kowatz T, Babino D, Kiser P, Palczewski K, von Lintig J, Characterization of human beta,beta-carotene-15,15'-monooxygenase (BCMO1) as a soluble monomeric enzyme, Arch. Biochem. Biophys, 539 (2013) 214–222. [PubMed: 23727499]

[94]. Kiser PD, Palczewski K, Membrane-binding and enzymatic properties of RPE65, Prog. Retin. Eye Res, 29 (2010) 428–442. [PubMed: 20304090]

[95]. Dela Sena C, Sun J, Narayanasamy S, Riedl KM, Yuan Y, Curley RW Jr., Schwartz SJ, Harrison EH, Substrate Specificity of Purified Recombinant Chicken beta-Carotene 9',10'-Oxygenase (BCO2), J. Biol. Chem, 291 (2016) 14609–14619. [PubMed: 27143479]

[96]. Hu KQ, Liu C, Ernst H, Krinsky NI, Russell RM, Wang XD, The biochemical characterization of ferret carotene-9',10'-monooxygenase catalyzing cleavage of carotenoids in vitro and in vivo, J. Biol. Chem, 281 (2006) 19327–19338. [PubMed: 16672231]

[97]. dela Sena C, Narayanasamy S, Riedl KM, Curley RW Jr., Schwartz SJ, Harrison EH, Substrate specificity of purified recombinant human beta-carotene 15,15'-oxygenase (BCO1), J. Biol. Chem, 288 (2013) 37094–37103. [PubMed: 24187135]

[98]. Lindqvist A, Andersson S, Biochemical properties of purified recombinant human beta-carotene 15,15'-monooxygenase, J. Biol. Chem, 277 (2002) 23942–23948. [PubMed: 11960992]

[99]. Wang X, Wang T, Jiao Y, von Lintig J, Montell C, Requirement for an enzymatic visual cycle in Drosophila, Curr. Biol, 20 (2010) 93–102. [PubMed: 20045325]

[100]. Babino D, Golczak M, Kiser PD, Wyss A, Palczewski K, von Lintig J, The Biochemical Basis of Vitamin A3 Production in Arthropod Vision, ACS Chem. Biol, 11 (2016) 1049–1057. [PubMed: 26811964]

[101]. Kiser PD, Zhang J, Badiee M, Li Q, Shi W, Sui X, Golczak M, Tochtrop GP, Palczewski K, Catalytic mechanism of a retinoid isomerase essential for vertebrate vision, Nat. Chem. Biol, 11 (2015) 409–415. [PubMed: 25894083]

[102]. Ronquist F, Huelsenbeck JP, MrBayes 3: Bayesian phylogenetic inference under mixed models, Bioinformatics, 19 (2003) 1572–1574. [PubMed: 12912839]

[103]. Sievers F, Wilm A, Dineen D, Gibson TJ, Karplus K, Li W, Lopez R, McWilliam H, Remmert M, Soding J, Thompson JD, Higgins DG, Fast, scalable generation of high-quality protein multiple sequence alignments using Clustal Omega, Mol. Syst. Biol, 7 (2011) 539. [PubMed: 21988835]

[104]. Pravda L, Sehnal D, Tousek D, Navratilova V, Bazgier V, Berka K, Svobodova Varekova R, Koca J, Otyepka M, MOLEonline: a web-based tool for analyzing channels, tunnels and pores (2018 update), Nucleic Acids Res., 46 (2018) W368–W373. [PubMed: 29718451]

[105]. Waterhouse A, Bertoni M, Bienert S, Studer G, Tauriello G, Gumienny R, Heer FT, de Beer TAP, Rempfer C, Bordoli L, Lepore R, Schwede T, SWISS-MODEL: homology modelling of protein structures and complexes, Nucleic Acids Res., 46 (2018) W296–W303. [PubMed: 29788355]

Highlights

- CCDs are iron-dependent, alkene-cleaving enzymes broadly found in nature
- Crystal structures for six distinct alkene-cleaving CCDs have been solved to date
- Universal and unique structural features of CCDs are described.
- CCD catalysis is discussed in light of recent experimental and computational studies

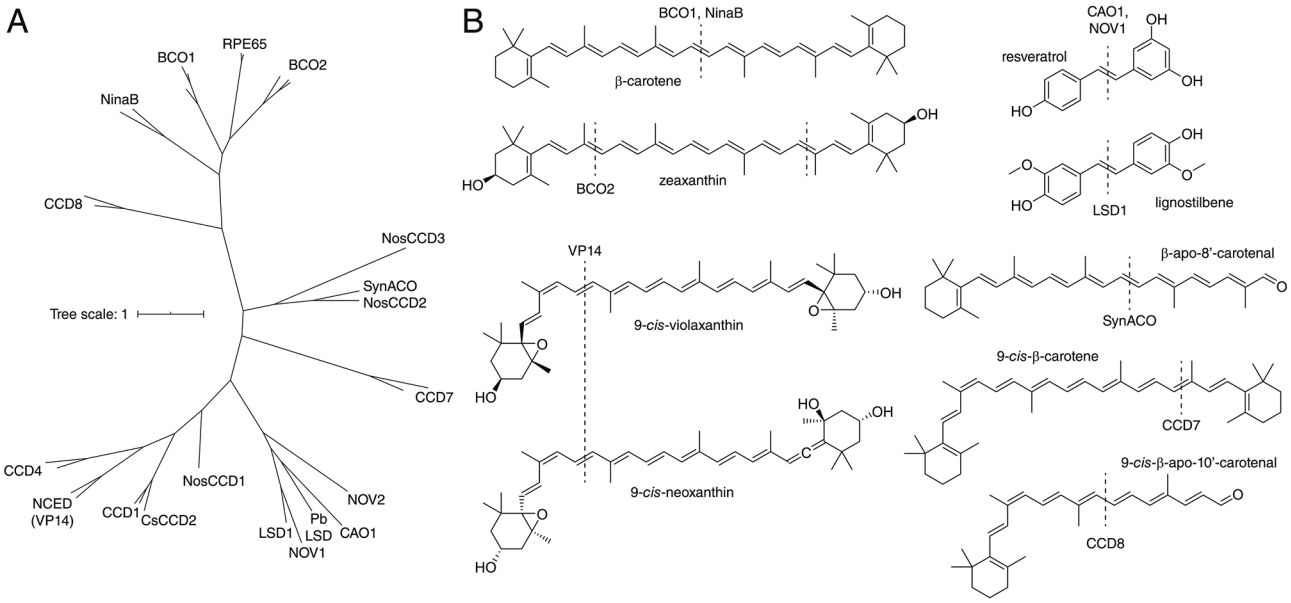

Figure 1. Phylogeny and cleavage specificity of CCDs.

A) Unrooted phylogenic tree of CCD protein sequences discussed in the main text. The tree was computed using MrBayes [102] based on a sequence alignment generated in Clustal Omega [103]. All bipartitions had posterior probabilities >90%. The scale represents average number of substitutions. Nos – *Nostoc*, Syn – *Synechocystis*, Pb – *Pseudomonas brassicacearum*. **B**) Cleavage site selectivity for CCDs and substrates discussed in the main text.

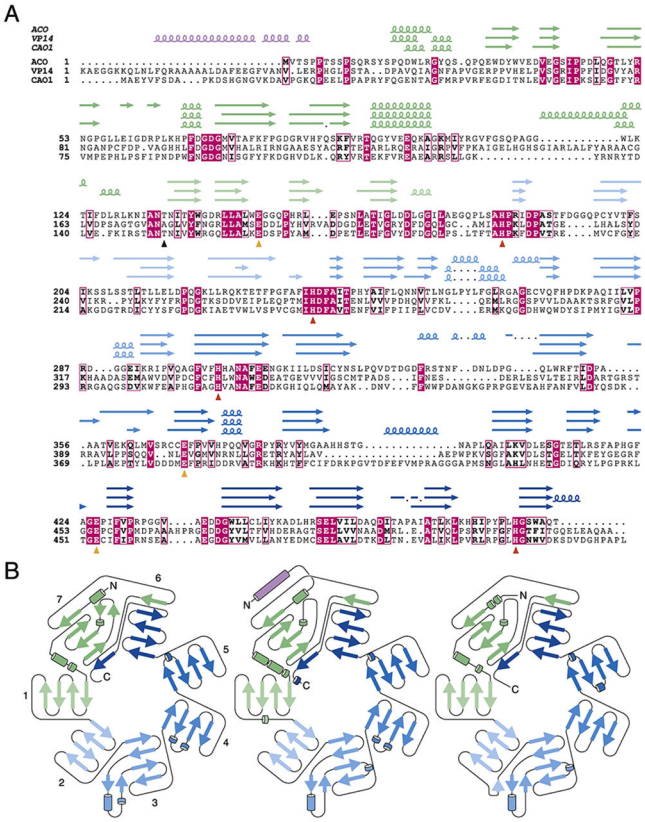

Figure 2. Sequence alignment and topology of ACO, VP14, and CAO1.

A) Sequence alignment and corresponding secondary structures determined by X-ray crystallography. The conserved iron-binding His and Glu residues are marked with red and orange triangles, respectively. The black triangle indicates residues in close proximity to the iron that appear to occlude in many CCDs, although not in VP14 due to the smaller Ala side chain. **B**) Topology diagrams for ACO [19] (left), VP14 [53] (middle), and CAO1 [43] (right). The blades are color-matched to the secondary structure elements shown in panel A.

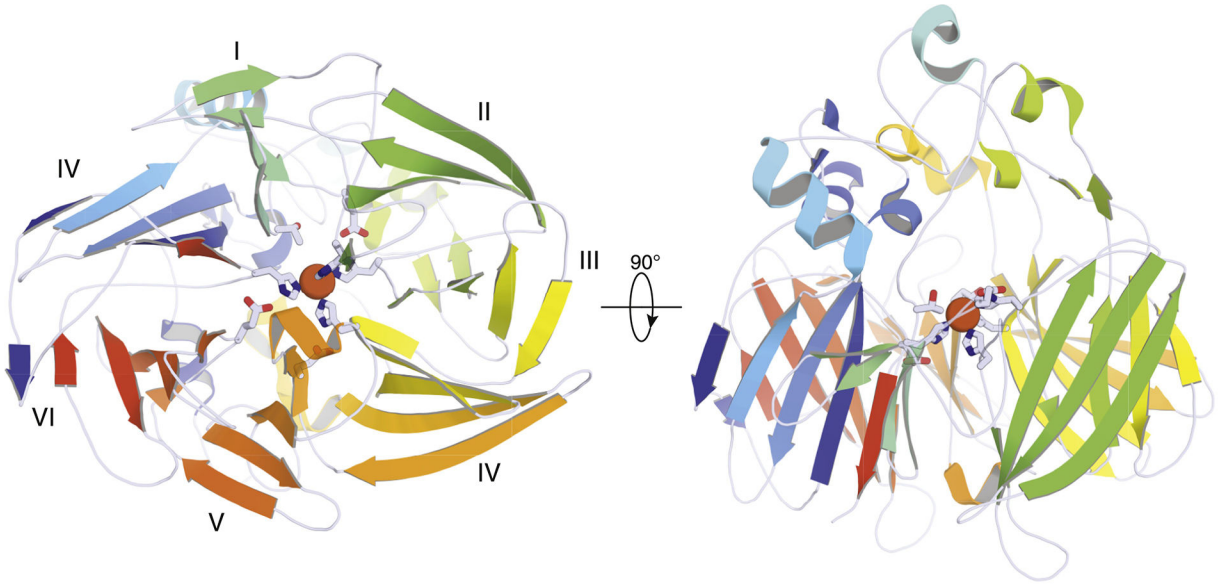

Figure 3. Crystal structure of ACO.

Cartoon representation showing the seven bladed beta-propeller structure capped by a cluster of helical segments that form a dome housing the active site [19]. The iron cofactor (brown sphere) is directly coordinated by four His residues, three of which are stabilized by hydrogen bonding with conserved Glu residues. All structural images were generated using PyMOL. This figure was adapted with permission from [33]. Copyright John Wiley & Sons, Ltd.

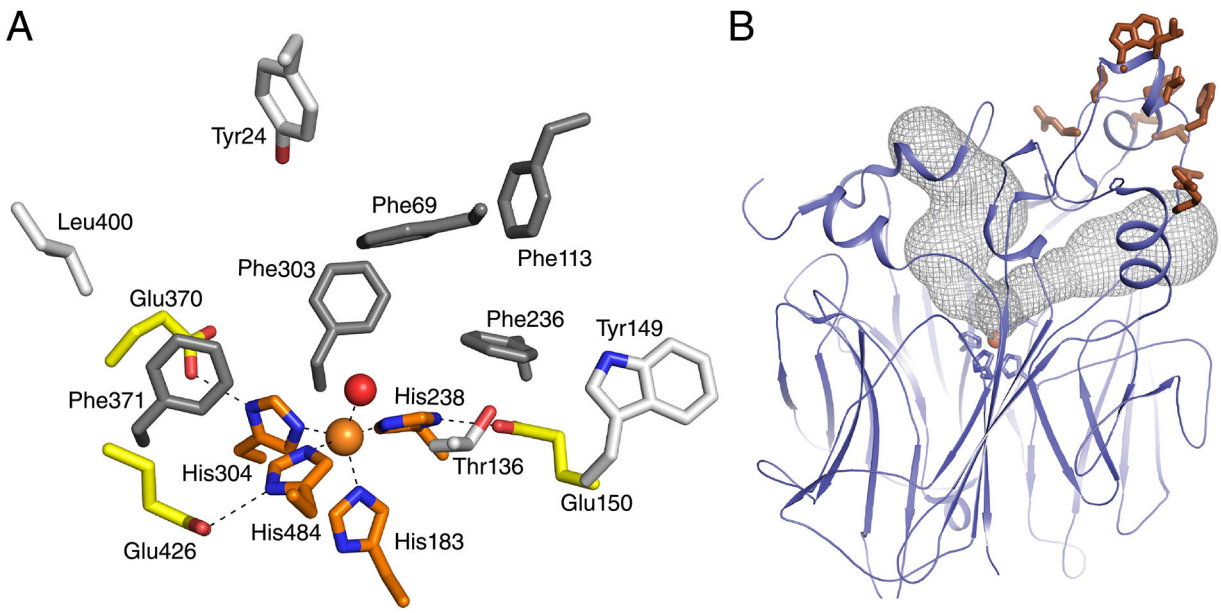

Figure 4. Active site of ACO.

A) Structure of the ACO active site [19]. The iron cofactor is shown as an orange sphere. An iron-bound solvent atom is shown as a red sphere. **B**) Tunnels leading to the iron center from the protein exterior. Residues thought to mediate membrane binding are shown as brown sticks. Substrate is presumably extracted from the membrane through the tunnel surrounded by the membrane-binding residues. Tunnels were generated using the MOLE*online* web interface [104].

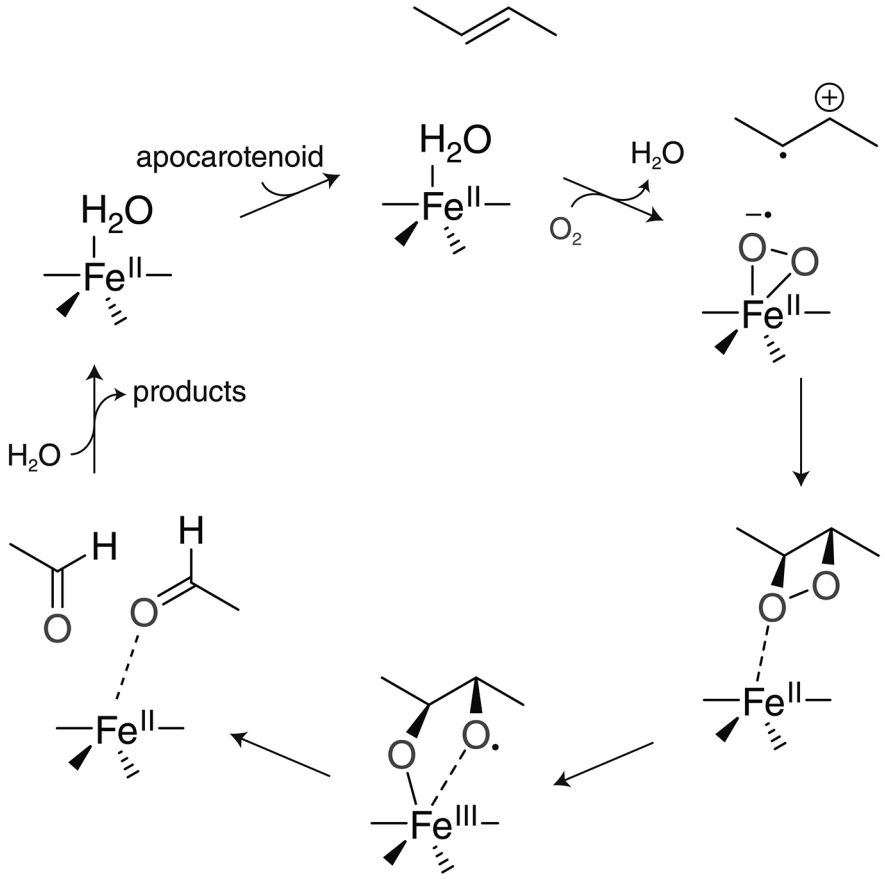

Figure 5. Proposed catalytic mechanism of ACO.

Only the scissile double bond and directly connected carbons are shown for simplicity. The mechanism is based on both computational and experimental results as described in the main text.

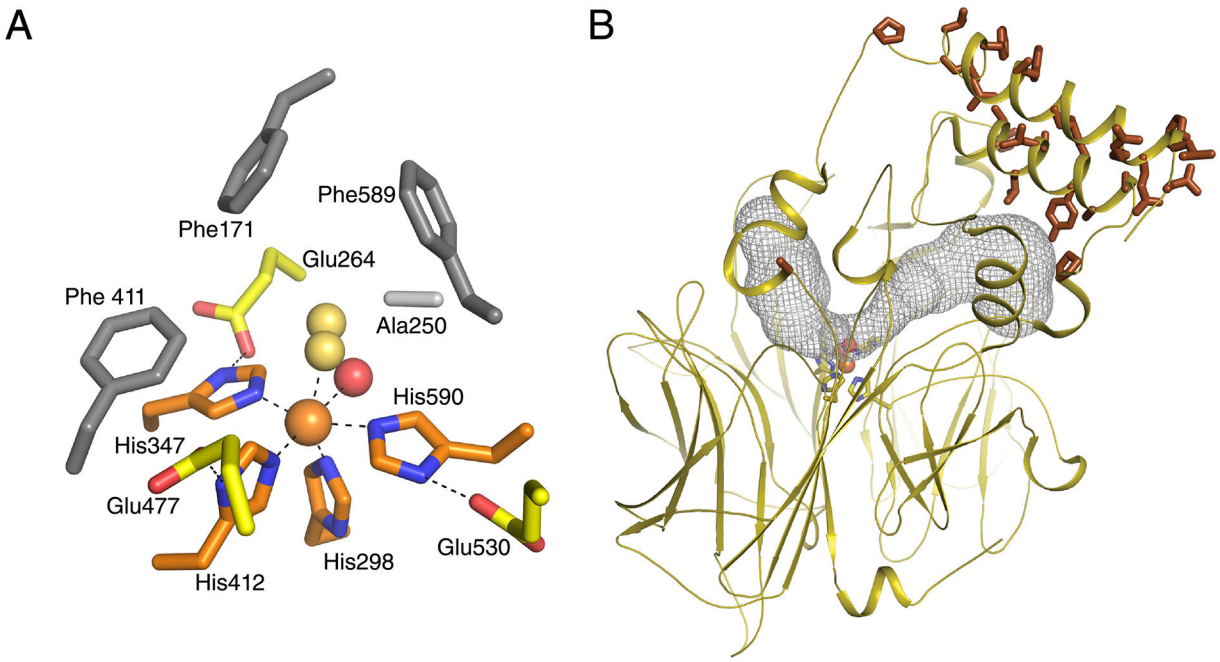

Figure 6. Active site of VP14.

A) Structure of the VP14 active site [53]. The iron cofactor is shown as an orange sphere. Iron-bound solvent and dioxygen are shown as red and gold spheres, respectively. **B**) Tunnels leading to the iron center from the protein exterior. Residues thought to mediate membrane binding are shown as brown sticks. Substrate is presumably extracted from the membrane through the tunnel surrounded by the membrane-binding residues.

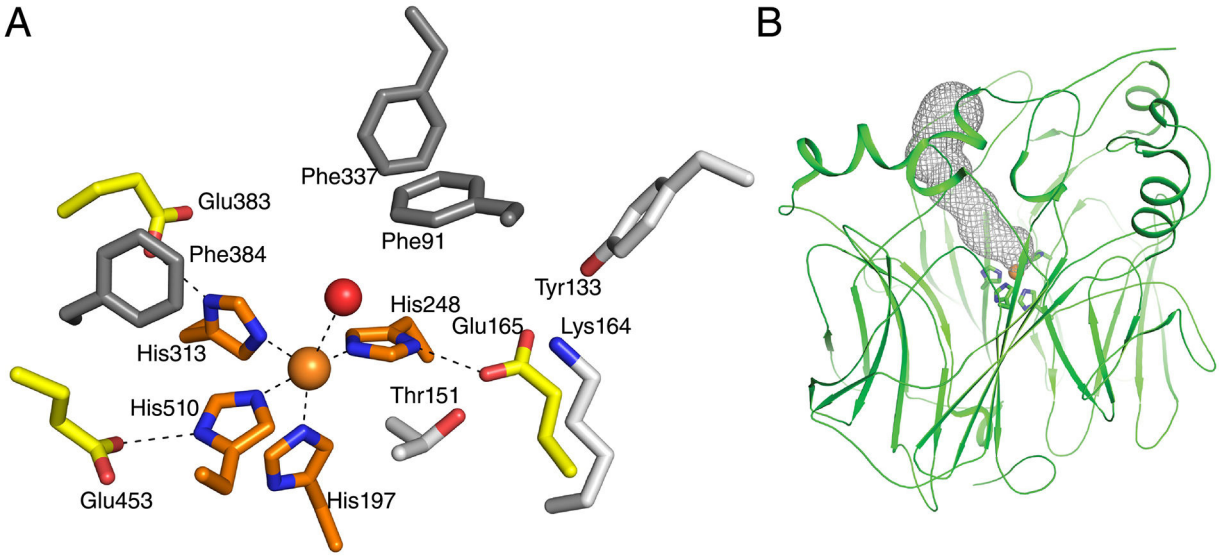

Figure 7. Active site of CAO1.

A) Structure of the CAO1 active site [43]. The iron cofactor is shown as an orange sphere. An iron-bound solvent atom is shown as a red sphere. **B**) A single tunnel leads to the iron center from the protein exterior. CAO1 and other stilbene-cleaving CCDs lack a hydrophobic patch that could mediate membrane binding.

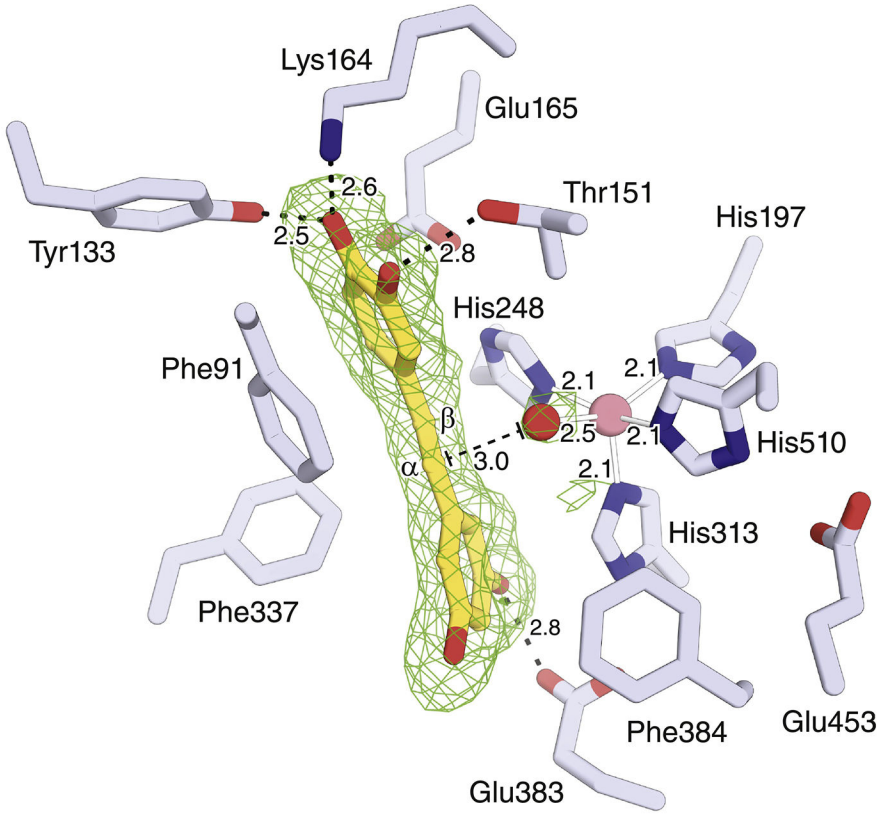

Figure 8. Structure of CAO1 in complex with piceatannol.

The structure was obtained by co-crystallizing piceatannol with Co-substituted CAO1, which is catalytically inactive [43]. The green mesh represents omit Fo-Fc electron density. Note the interaction of the 4-hydroxy group with Lys164 and Tyr133, both of which are important for catalytic function. This figure was adapted with permission from [33]. Copyright John Wiley & Sons, Ltd.

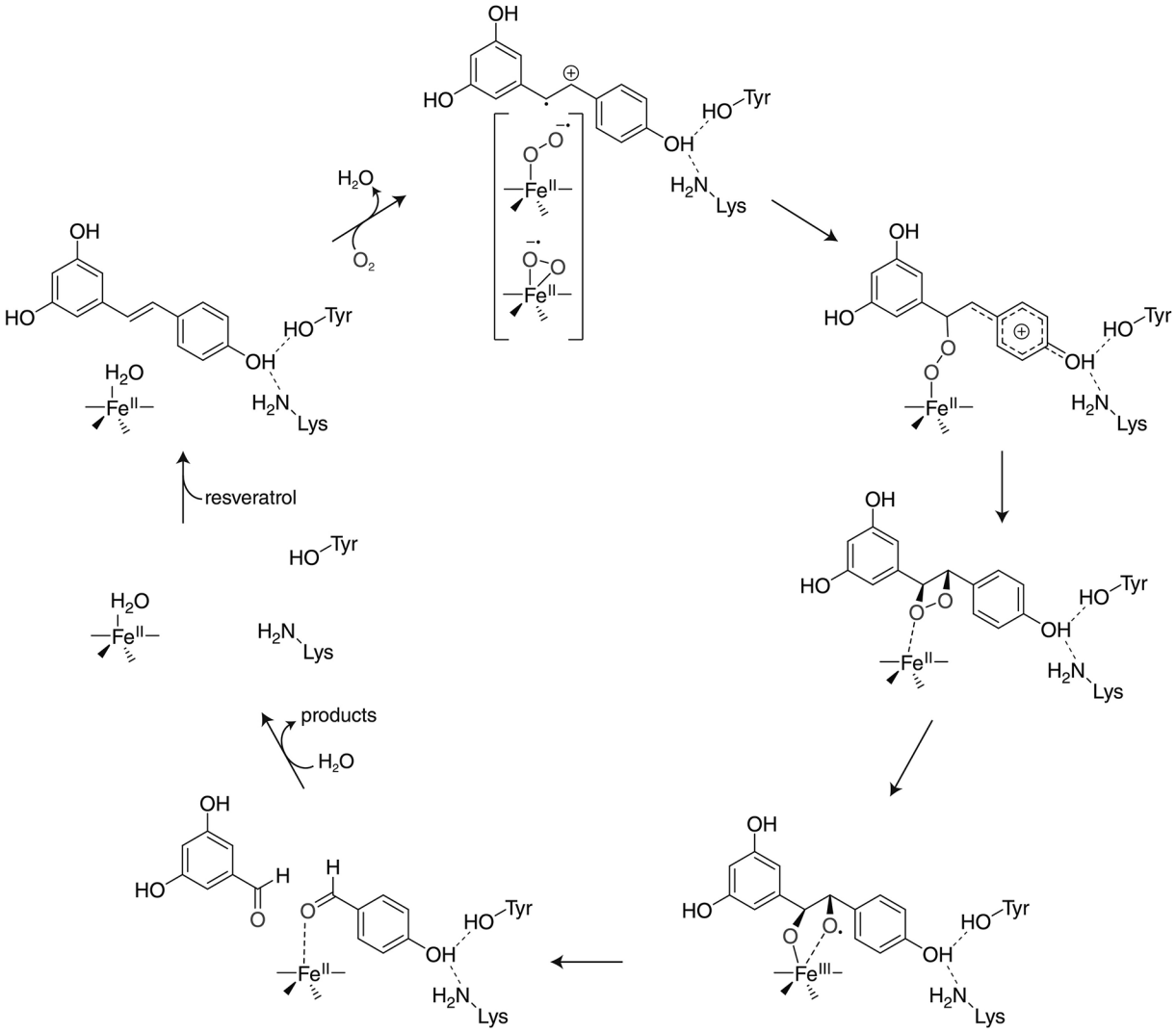

Figure 9. Proposed catalytic mechanism of stilbene-cleaving CCDs.

The mechanism is based on both computational and experimental results as described in the main text.

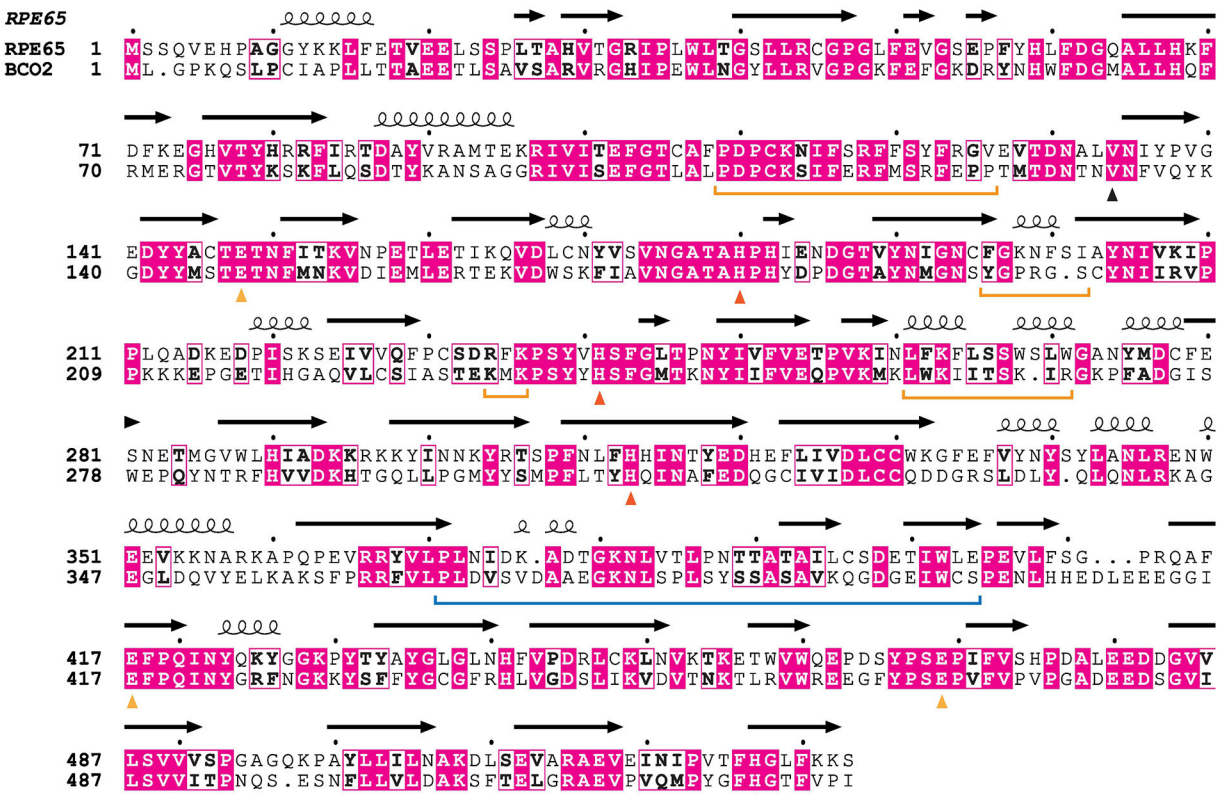

Figure 10. Sequence alignment between bovine RPE65 and mouse BCO2.

Secondary structure for RPE65 determined by crystallography is shown above the alignment. Residues thought to mediate membrane binding of these proteins are marked by horizontal orange brackets. The region mediating dimer formation in RPE65 is marked by a horizontal blue bracket. The conserved metal-binding His and Glu residues are marked by red and orange triangles, respectively, while the occluding Val residue is marked by a black triangle.

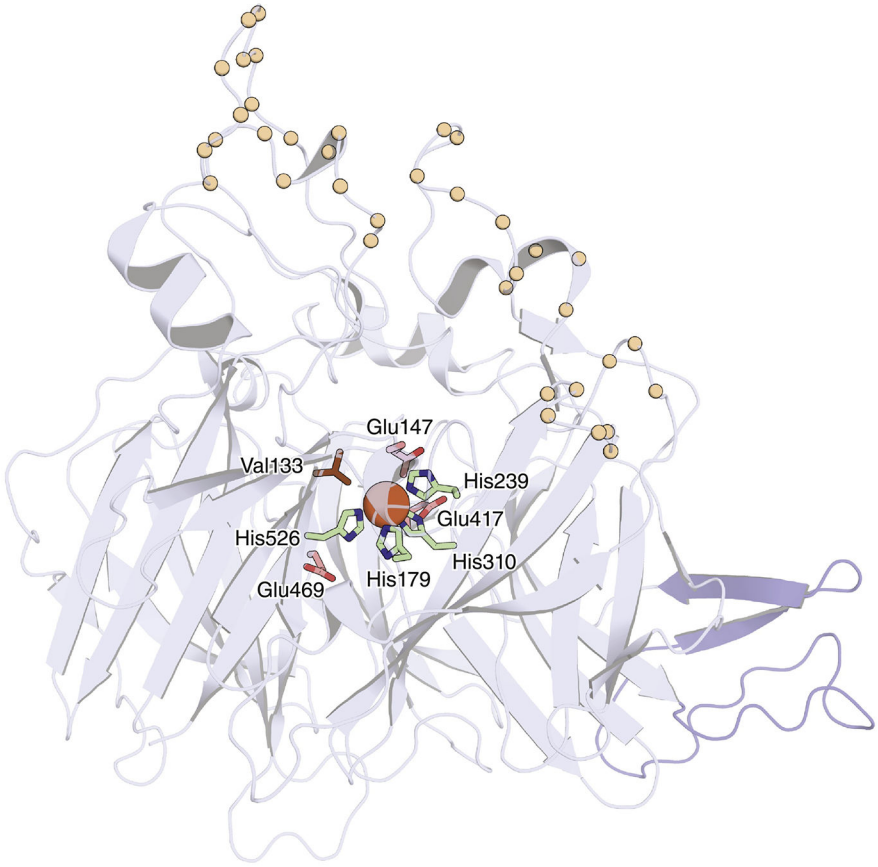

Figure 11. Homology model of mouse BCO2.

The model was generated by the SwissModel server [105] using the crystallographic coordinates of RPE65 [91]. Residues that likely mediate membrane affinity in this protein are marked by pale orange spheres. The loop that may mediate dimer formation is colored blue. Key active site residues are shown as sticks and the iron cofactor is shown as a dark orange sphere.